JGR Oceans

RESEARCH ARTICLE
10.1029/2023JC019821

Special Section:
Physical and biogeochemical processes affecting nutrients and the carbon cycle in mesoscale eddies of subtropical oceans

Dissolved Organic Matter Fluorescence as a Tracer of Upwelling and Microbial Activities in Two Cyclonic Eddies in the Eastern Tropical North Atlantic

Quentin Devresse[1], Kevin W. Becker[1], Ahmad Fehmi Dilmahamod[1], Eva Ortega-Retuerta[2], and Anja Engel[1]

[1]GEOMAR Helmholtz Centre for Ocean Research Kiel, Kiel, Germany, [2]CNRS/Sorbonne Université, UMR7621 Laboratoire d'Océanographie Microbienne, Banyuls sur Mer, France

Key Points:

- Four fluorescent dissolved organic matter (FDOM) components were studied in two cyclonic eddies (CEs) in the Eastern Tropical North Atlantic
- Tryptophan-like FDOM was an indicator of the CEs' productivity as it correlated with semi-labile dissolved organic matter and microbial metabolic activities
- Humic-like FDOM was a by-product of microbial respiration; its distribution within an offshore CE covaried with nutrient upwelling

Supporting Information:

Supporting Information may be found in the online version of this article.

Correspondence to:

A. Engel,
aengel@geomar.de

Citation:

Devresse, Q., Becker, K. W., Dilmahamod, A. F., Ortega-Retuerta, E., & Engel, A. (2023). Dissolved organic matter fluorescence as a tracer of upwelling and microbial activities in two cyclonic eddies in the Eastern Tropical North Atlantic. *Journal of Geophysical Research: Oceans*, *128*, e2023JC019821. https://doi.org/10.1029/2023JC019821

Received 9 MAR 2023
Accepted 3 AUG 2023

Abstract Mesoscale eddies are frequently observed in the Eastern Tropical North Atlantic (ETNA), yet their effects on the transport and distribution of biogeochemical solutes, and specifically on the production and remineralization of dissolved organic matter (DOM) remain difficult to elucidate. Here, we investigated the submesoscale variability of chromophoric DOM (CDOM) and fluorescent DOM (FDOM) together with microbial production and remineralization processes in two cyclonic eddies (CEs) in the ETNA during summer and winter 2019. One CE, formed near the coast off Mauritania during the post-upwelling season, was sampled along a ~900 km zonal corridor between Mauritania and the Cape Verde Islands. The other CE, formed nearby Brava Island, was out of coastal influence. Four fluorescent components were identified with parallel factor analysis, two humic-like, and two protein-like components. Humic-like FDOM components correlated to optode-based community respiration and were also good indicators of upwelling associated with the Brava Island CE as they correlated to physical parameters (e.g., temperature) and to dissolved inorganic nitrogen. The tryptophan-like FDOM components correlated with the carbon and nitrogen content of semi-labile DOM, phytoplankton biomass, community respiration, and bacterial production. Overall, our study revealed that DOM optical properties are suitable for tracing freshly produced organic matter and the transport of remineralized DOM within offshore eddies.

Plain Language Summary Mesoscale eddies are ubiquitous circulation features in the ocean with horizontal scales on the order of 100 km and lifetimes of days to months. Their swirling motion can cause nutrients from deeper waters to be transported to the surface, stimulating phytoplankton biomass and resulting in the production of dissolved organic matter. However, these effects are difficult to quantify and proxies (biomarkers) are needed to monitor the impact of eddies at high resolution. In this work, we used the optical properties of the dissolved organic matter, especially the fraction capable of fluorescence (FDOM) as biomarker in two cyclonic eddies, one formed in an eastern boundary upwelling system and one formed offshore by winds/Island interaction. We identified four FDOM components, among which an indicator of cyclonic eddy productivity and two indicators of dissolved organic matter recycling, which also tracked nutrient transport in the offshore cyclonic eddy. Our study highlights that continuous FDOM data obtained with sensors could help to follow eddy development and influence on seawater biogeochemistry.

1. Introduction

Mesoscale eddies are ubiquitous in the global ocean, with horizontal scales on the order of 10^2 km. Eddies host water masses of unique characteristics, which are trapped within their cores and subsequently transported with them along their trajectories (e.g., Goni & Johns, 2001; Witter & Gordon, 1999). With a lifespan from days to months, they can travel several hundred to thousands of kilometers across ocean basins (Chelton et al., 2011). Based on the rotation direction of the eddy flow field and their vertical structure, three different types of eddies have been identified: cyclonic (CEs), anticyclonic (ACEs), and anticyclonic mode water eddies (ACMEs) (Chelton et al., 2011; D'Asaro, 1988). Different dynamical mechanisms can explain the generation of mesoscale eddies, among which are the mean flow separation along slope boundary currents at sharp topographic headlands (coastal eddies) in Eastern Boundary Upwelling Systems (EBUS) (D'Asaro, 1988; Dilmahamod et al., 2022; Molemaker et al., 2015; Thomsen et al., 2016), or by wind island-topography interaction (Island eddies; Chavanne et al., 2002). Depending on their polarity, eddies can cause pycno-, thermo-, and nutriclines to dome upward or

downward (see review by McGillicuddy, 2016). Eddies are crucial vectors modulating oceanic biogeochemical variability on a basin scale because they might transport nutrients and organic carbon from EBUS to the open ocean (Garçon et al., 2001). A better understanding of eddy dynamics and how they affect their surrounding environment is needed to assess and predict biogeochemical processes in the ocean accurately. Earth system models used to project future global biogeochemical cycling often do not resolve mesoscale eddies, leading to uncertainties in estimating, for example, net primary production (PP; Bonan & Doney, 2018; Couespel et al., 2021; Gent & McWilliams, 1990). In the subtropical gyres of the World's oceans, inorganic nutrients (e.g., nitrate or phosphate) limit microbial activities of dissolved organic matter (DOM) production and degradation (Alonso-Sáez et al., 2007; Moore et al., 2013; Romera-Castillo et al., 2016). Eddies, through their passages, might suppress those limitations and enhance microbial activities (Devresse et al., 2022; Ewart et al., 2008). The phytoplankton response to nutrient is nonlinear, with a lag phase with a lag phase of 1–3 days between uptake of nutrients and plankton bloom (e.g., Collos, 1986; Wetz & Wheeler, 2004). Additionally, the advection of phytoplankton cells by the flow associated with eddy motion and westward propagation creates a nonuniform distribution of phytoplankton within eddies (Chelton et al., 2011; McGillicuddy, 2016). These factors altogether create spatial variability at the submesoscale (<10 km) within eddies of phytoplankton biomass, communities, and primary productivity (Belkin et al., 2022; Bibby et al., 2008; Devresse et al., 2022; Lochte & Pfannkuche, 1987; Singh et al., 2015). Bacterial activity is directly coupled to primary productivity as autotrophic cells release their main substrate DOM. Consequently, heterotrophic bacteria biomass, communities, and microbial consumption of organic matter (community respiration, bacterial respiration, and production) also vary within eddies (Devresse et al., 2022; Ewart et al., 2008; Mouriño-Carballido, 2009; Mouriño-Carballido & McGillicuddy, 2006; Yan et al., 2018). The problem is that the effects of eddies are quantifiable through discrete sampling and bottle-incubations that are time-consuming making difficult to establish the high-resolution impact of eddies on organic matter turnover. Optical sensors mounted on gliders, floats, or attached to rosettes could help improve high-resolution analysis of eddies. However, this requires extensive knowledge of DOM optical properties within eddies.

Chromophoric DOM (CDOM) is absorbing in the UV-visible radiation (200–780 nm) range (Coble, 2007), and fluorescent DOM (FDOM) is emitting fluorescence. Optical analyses (i.e., absorption and fluorescence) of DOM are widely applied to characterize the sources, transport and transformation dynamics of CDOM and FDOM (see reviews by Nelson & Siegel, 2013; Li & Hur, 2017). Excitation and Emission spectra of FDOM through the application of parallel factor analysis (PARAFAC) have been used to distinguish different DOM pools (e.g., Stedmon & Bro, 2008). FDOM components that are excited in the UV spectral range but emit in the UV A-visible spectral (315–700 nm) are usually indicative of fulvic- and humic-like DOM compounds (Coble, 1996; Guéguen & Kowalczuk, 2013) and have been related to semi-refractory or refractory compounds (Catalá et al., 2015). FDOM components that are excited and emit in the UV spectral range commonly correspond to labile proteinaceous/freshly produced DOM and comprise protein-like DOM (Yamashita & Tanoue, 2003). Nevertheless, previous studies have shown that other non-protein-like compounds can also fluoresce in low-UV regions (Coble, 2007; Hernes & Benner, 2003). CDOM absorption coefficients in the UV A fraction (315−400 nm) and fulvic/humic FDOM components generally increase with depth in the open ocean (Jørgensen et al., 2011; Kowalczuk et al., 2013; see review by Nelson & Siegel, 2013; Catalá et al., 2015) and decrease due to photodegradation (e.g., Helms et al., 2013). Both CDOM and FDOM have been used to track water mass transport and biogeochemical processes in upwelling areas, such as the Iberian Peninsula (Nieto-Cid et al., 2006), the Peruvian (Engel & Galgani, 2016; Loginova et al., 2016) and the Mauritanian (Heller et al., 2016) upwelling systems. An increase in humic-like FDOM associated with microbial remineralization (i.e., apparent oxygen utilization) and an increase in protein-like FDOM associated with nutrient transport have been observed in CEs in the South China Sea (Wang et al., 2017; M. Zhang et al., 2020; Y. Zhang et al., 2009) and in the Bay of Bengal, respectively (Chiranjeevulu et al., 2014). However, studies using the optical properties of DOM as tools to investigate coastal-open ocean interactions mediated by eddies are still very limited.

Here, we studied CDOM and FDOM at high spatial resolution in and around two CEs (coastal and island CEs) in the Mauritania Upwelling System (13°−20°N) in 2019. In this region, about ∼150 eddies with a lifetime of more than 7 days are generated per year (Schütte et al., 2016). We determined DOM optical properties (CDOM and FDOM) and linked them to DOM quality (lability) and quantity, microbial metabolic activities including PP, community respiration, and bacterial production, autotrophic plankton biomass (Chlorophyll-*a*), as well as heterotrophic bacterial and viral abundances. Our study provides new insights into how cyclonic eddies (CEs), in which nutrients are upwelled and transported from the coast to the open ocean, affect DOM production and remineralization, and how DOM optical properties can be used to discern those processes.

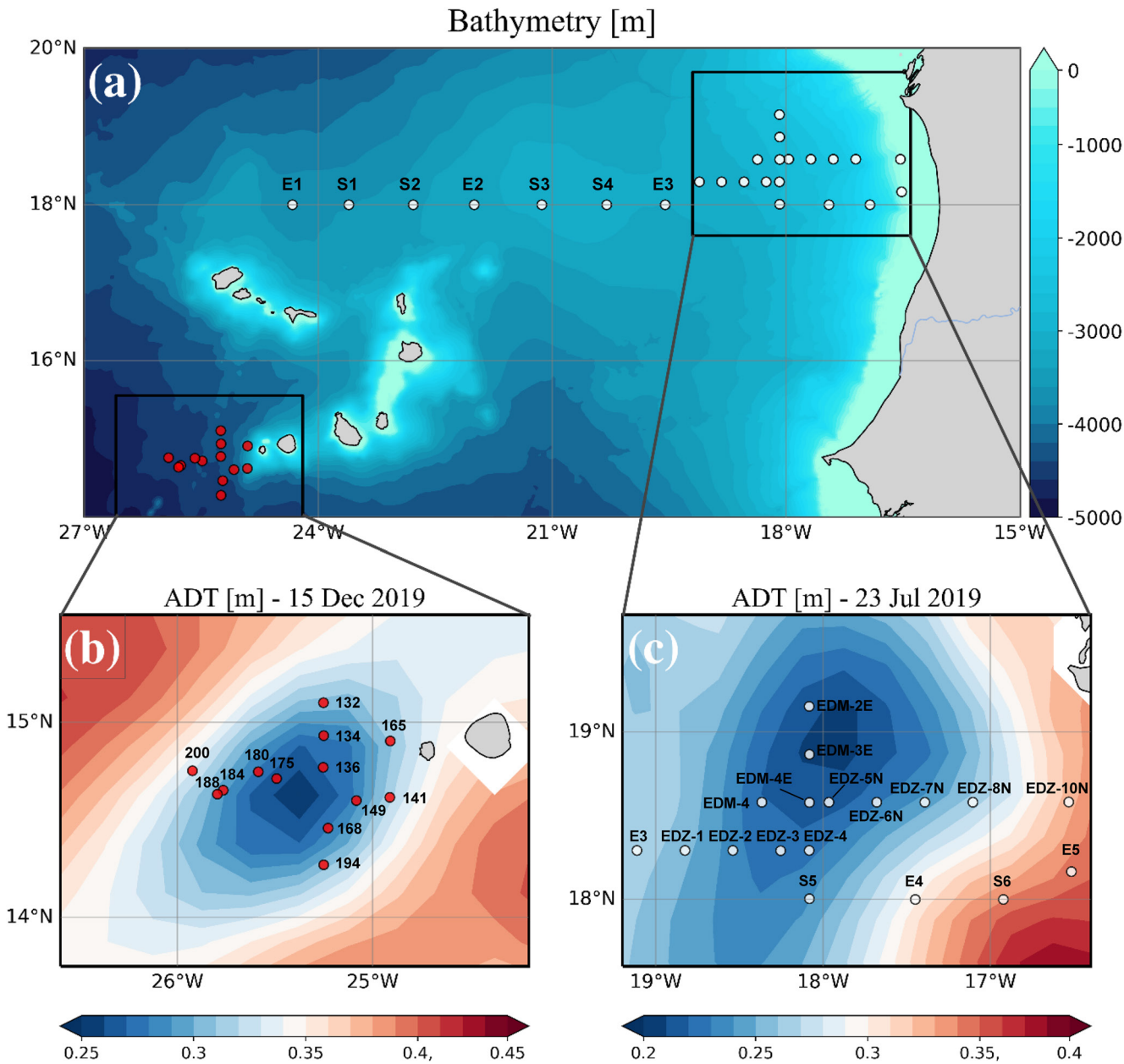

Figure 1. Sampling stations during RV *Meteor* cruises M156 (white dots) and M160 (red dots) (a), with zoom-in into the Brava eddy (b) and Mau eddy (c). The background in (b and c) shows the gridded absolute dynamic topography (ADT) obtained from AVISO.

2. Materials and Methods

2.1. Study Area, Sampling Strategy and Eddy Characterization

Sampling was conducted in the Eastern Tropical North Atlantic in the vicinity of the Cape Verde archipelago and the Mauritanian coast during the R/V *Meteor* cruises M156 (3 July to 1 August 2019) and M160 (22 November to 20 December 2019). During the cruises, two eddies of distinct origins and lifespan were sampled at high spatial resolution. Sea surface height and acoustic Doppler current profiler (ADCP) velocity data characterized the two eddies as CEs. The first CE (Mau eddy) was sampled in summer 20 km offshore the Mauritanian Coast during M156 along two zonal transects (19.1°W−18.2°W at 18.3°N and 18.5°W−17.1°W at 18.6°N) and one meridional transect (19.4°N−18°N at 18.4°W–18.1°W). In addition, we sampled water along an 18°N transect, a typical coast-to-open ocean trajectory of eddies in this region (Devresse et al., 2022; Schütte et al., 2016; Figure 1). The second CE was

sampled in winter during the cruise M160, in the vicinity of Brava Island (Brava eddy). Here, we also sampled along a zonal transect (25.9°W−24.9°W at 14.8°N–14.6°N) and a meridional transect (15.1°N−14.2°N at 25.3°W; Figure 1).

Salinity, temperature, depth, and O_2 concentration were determined using a Seabird 911 plus CTD system equipped with two independently working sets of CTD sensors. The oxygen sensor was calibrated against discrete water samples using the Winkler method (Strickland & Parsons, 1968; Winkler, 1888). Seawater samples were collected using 10 L Niskin bottles attached to the CTD Rosette. During M156, 25 stations were sampled; with 14 of them inside or in the vicinity of the Mau eddy. During M160, 12 stations were sampled, with four of them inside or in the vicinity of the Brava eddy. Sampling was conducted in the epipelagic layer (0−200 m), including samples from the surface mixed layer, the Chl-*a* maximum, and the shallow oxygen minimum zone (<50 μmol kg^{-1} between 0 and 200 m depth), if present. Analysis of eddy statistics from an eddy detection and tracking algorithm (Le Vu et al., 2018) showed that both CEs were 1.5 months old.

Determining eddy peripheries is difficult, with satellite altimetry and sea surface temperature providing some insights, but often not enough to locate eddies for dedicated biogeochemical sampling (Figure S1 in Supporting Information S1). For this reason, we combined different approaches to define eddy structures as the area influenced by eddies. For the Mau eddy, we used the same border as described in details in Devresse et al. (2022), and for the Brava eddy, we used surface temperature, salinity, and Chl-*a* data through high-resolution sampling to approximate eddies' periphery as the area influenced by eddies. During M156, the Mau eddy center was located at 18.69°N−18.05°W, on 22 July 2019, with a core radius of 40.5 ± 5.7 km and a mean azimuthal velocity of 19.9 ± 0.7 cm s^{-1}. Stations outside and westward of the eddy influence were referred to as "open ocean" and those close to the coast as "coastal." Just beyond the eddy periphery, at St. E3, a front was observed with surface temperature and salinity (not compensated by density) different from the adjacent stations (Devresse et al., 2022). Hence, we referred to that station as "Frontal Zone." During M160, the Brava eddy had an elliptic shape and its center and core radius could not be realistically determined by vmADCP reconstruction and were instead determined from mini-drifter (Carrasco et al., 2020; Fischer et al., 2021). The Brava eddy center was located at 14.5°N, 25.5°W, on 13 December 2019.

2.2. Water Mass Analysis

The two extremes along-isopycnals (fresh and cold vs. warm and saline) in the region separate the dominant water masses, namely South Atlantic Central Water (SACW) and North Atlantic Central Water (NACW). A simple water mass analysis accounting for endmember mixing along isopycnals (Dilmahamod et al., 2022; Klenz et al., 2018) was performed to investigate the % of SACW during the cruises. As in Klenz et al. (2018), lower and higher salinity and temperature bounds were chosen for SACW (35.1°C−35.65°C; 9.6°C−17.9°C) and NACW (35.37°C−37°C; 10.8°C−21.8°C), from which relative contributions of SACW was calculated. However, it is important to note that the water mass analysis determined through this method should be considered as relative contributions to a specific water sample, and the outcome can vary based on the salinity and potential temperature limits selected for the analysis.

2.3. Chemical and Biological Analyses

2.3.1. Measurements of Absorption and Fluorescence of Dissolved Organic Matter

Samples (40 mL) were collected into combusted (450°C, 8 hr) amber-glass vials after filtering through polyethersulfone syringe filters with 0.2 μm pore size (CHROMAPHIL® Xtra PES-45/25, MACHEREY-NAGEL GmbH & Co.KG) and stored at 4°C in the dark. Syringes were rinsed with 25 mL of mili-Q and filters with 50 mL of mili-Q and 5 mL of sample in order to remove potential contaminations. Samples were brought to room temperature (~20°C) before analyses and analyzed within 9 months after the cruises. The CDOM absorbance was measured with a Shimadzu® 1800 UV-VIS double beam spectrophotometer using a 10 cm Quartz SUPRASILVR precision cell (Hellma® Analytics) at 1 nm wavelengths intervals from 230 to 750 nm against Milli-Q water as a reference. Instrumental absorbance baseline drift was corrected by subtracting the mean of the absorbance between 680 and 700 nm (Li & Hur, 2017). CDOM absorbance spectra were converted to absorption coefficients according to Bricaud et al. (1981):

$$a_{\mathrm{CDOM}}(\lambda) = \frac{2.303A(\lambda)}{L} \quad (1)$$

where $a_{CDOM}(\lambda)$ is the absorption coefficient at wavelength λ (m^{-1}), $A(\lambda)$ is the absorbance value at the same wavelength and L is the effective optical path length (m). Absorption at 325 nm ($a_{CDOM}(325)$) was used as a proxy for open ocean CDOM concentrations (Nelson & Siegel, 2013).

For the determination of FDOM, 3D-EEM fluorescence spectroscopy was performed using a Cary Eclipse Fluorescence Spectrophotometer (Agilent Technologies) equipped with a xenon flash lamp. The fluorescence spectra for samples were measured in a four-optical window 1 cm Quartz SUPRASIL® precision cell (Hellma® Analytics). Blank-3D fluorescence spectra were performed daily using an Ultra-Pure Water Standard sealed cuvette (3/Q/10/WATER; Starna Scientific Ltd). The experimental wavelength range for sample and ultra-pure water scans was 230–455 nm in 5 nm intervals on excitation and 290–700 nm in 2 nm intervals on emission. All fluorescence measurements were conducted at 20°C, controlled by Cary Single Cell Peltier Accessory (VARIAN), PMT 900V, 0.2 s integration times and 5 nm slit width on excitation and emission monochromators. The Ex/Em scans were later cut to intervals from 230 to 455 nm for excitation and from 290 to 500 nm for emission in order to reduce potential noise during PARAFAC analysis.

All calculations were conducted using the software R (v4.0.2.) in RStudio (v1.1.414; Ihaka & Gentleman, 1996) with the package staRdom ("spectroscopic analysis of DOM in R") (Pucher et al., 2019). The 3D fluorescence spectra were corrected for spectral bias, background signals, and inner filter effects (Pucher et al., 2019 and references therein). Each EEM was normalized to the area of the ultra-pure water Raman peaks, measured on the same day. EEMs were combined into a four-dimensional data array and analyzed by PARAFAC (Stedmon & Bro, 2008). Determination of the most suitable number of components was achieved by the split-half analysis. Here, we report the maximum fluorescence (F_{max}) in Raman units (RUs) (Coble, 1996; Murphy et al., 2010; Stedmon et al., 2003).

2.3.2. Apparent Oxygen Utilization

The apparent oxygen utilization (AOU) was calculated as the difference between saturation concentrations of O_2 and measured O_2 concentrations: AOU = $[O_2{}^{sat}(\theta, S)] - [O_2]$, with S = salinity and θ = potential temperature (Pytkowicz, 1971; Redfield, 1942; Redfield et al., 1963). The saturated oxygen ($O_2{}^{sat}$) was computed using measured temperature and salinity following Garcia and Gordon (1992).

2.3.3. Inorganic Nutrients

Nutrient concentrations were measured onboard in duplicates from unfiltered seawater samples (11 mL). Phosphate ($PO_4{}^{3-}$), nitrate ($NO_3{}^-$), and nitrite ($NO_2{}^-$) were measured photometrically with continuous-flow analysis on an auto-analyzer (QuAAtro; Seal Analytical) after Grasshoff et al. (1999). Detection limits for $PO_4{}^{3-}$, $NO_3{}^-$, and $NO_2{}^-$ were 0.02, 0.1, and 0.02 µmol L^{-1}, respectively, for M156 and 0.01 µmol L^{-1} for $PO_4{}^{3-}$, $NO_3{}^-$, and $NO_2{}^-$ for M160. Dissolved inorganic nitrogen (DIN) was determined as the sum of $NO_3{}^-$ and $NO_2{}^-$, which did not include ammonium ($NH_4{}^+$).

2.3.4. Semi-Labile Dissolved Organic Matter

We determined high-molecular-weight (HMW >1 kDa) dissolved combined carbohydrates (dCCHO) and dissolved hydrolyzable amino acids (dHAA) as the main biochemical components of DOM (Carlson, 2002). For dCCHO and dHAA analyses, duplicate samples (20 mL) were filtered through 0.45 µm Acrodisk filters, collected in combusted glass vials, and frozen (−20°C) until analysis. dCCHO samples were desalted by membrane dialysis (1 kDa, Spectra Por) which exclude polysaccharides <1 kDa, oligosaccharides, and monosaccharides. After desalination, samples were hydrolyzed with hydrochloric acid and analyzed with high-performance anion exchange chromatography coupled with pulsed amperometric detection (HPAEC-PAD) (DIONEX ICS3000DC) after Engel et al. (2011) with a detection limit (DL) of 1 µg L^{-1}. The analysis detected 11 monomers: arabinose, fucose, galactose, galactosamine, galacturonic acid, glucosamine, glucose, glucuronic acid, rhamnose, co-elute mannose, and xylose. For dHAA, samples were measured by high-performance liquid chromatography (HPLC; Agilent Technologies, USA) and detected fluorometrically after hydrolysis at 100°C for 20 hr with hydrochloric acid (Suprapur, Merck), neutralization and in-line ortho-phthaldialdehyde derivatization with mercaptoethanol. The HPLC was equipped with a C_{18} column (2.6 µm, 4.6 × 150 mm, Phenomenex, USA) (Dittmar et al., 2009; Lindroth & Mopper, 1979). The analysis classified 13 monomers with a precision <5% and a DL of 2 nmol L^{-1}: alanine, arginine, aspartic acid, isoleucine, glutamic acid, glycine, leucine, phenylalanine, serine, threonine, tyrosine, valine, and γ-aminobutyric acid (GABA). The calculations for the carbon and nitrogen content of

dCCHO and dHAA were based on carbon and nitrogen atoms contained in the identified monomers. Combined forms of amino acids and carbohydrates are among the most reactive components of marine DOM (Benner & Amon, 2015). Hydrolyzable HMW compounds have varying lability and can be defined as labile or semi-labile with degradation time from hours to month (Carlson & Hansell, 2015, and references therein). Here, the sum of dCCHO and dHAA carbon and nitrogen contents are referred to as semi-labile dissolved organic carbon (SL-DOC) and nitrogen (SL-DON), respectively.

2.3.5. Dissolved Organic Matter

Duplicate samples for DOC and dissolved organic nitrogen (DON) were filtered through 0.45 µm GMF GD/X filters (Whatman, GE Healthcare Life Sciences, UK) and collected in combusted glass ampoules. Syringes and filters were rinsed with 25 and 50 mL of sample, respectively in order to remove potential contaminations. Samples were acidified with 20 µL of hydrochloric acid (30%) and stored at 4°C. DOC was analyzed by high-temperature combustion using a Shimadzu TOC-VCSH after Engel and Galgani (2016) and total dissolved nitrogen (TDN) was measured in parallel with a TNM-1 detector of the Shimadzu analyzer (Dickson et al., 2007) with a DL of 1 µmol L^{-1}. Every measurement day, ultrapure (MilliQ) water was used to determine the instrument blank, which was accepted for values <1 µmol C L^{-1} and <1 µmol N L^{-1}. TOC and TN analysis were validated on every measurement day with deep seawater reference material provided by the Consensus Reference Materials Project of RSMAS (University of Miami) yielding values within the certified range of 44–46 µmol C L^{-1} and 31–33 < 1 µmol N L^{-1}. Additionally, on each measurement day, we used two internal standards from potassium hydrogen phthalate (Merck 109017) and potassium nitrate (Merck 105065) standard solutions with DOC and TDN concentrations within the range of those in samples. Values of TDN were corrected with DIN and thereafter referred to as DON.

2.3.6. Chlorophyll-*a*

During the M156 cruise, 1 L samples were collected on 25 mm GF/F (Whatman, GE Healthcare Life Sciences, UK) for Chl-*a*. The samples were stored frozen (−20°C) until extraction using 90% acetone for photometric analyses (Turner Designs, USA), slightly modified after Evans et al. (1987). During M160, Chl-*a* was determined from a modified version of the method described in Garrido et al. (2003). The concentration of Chl-*a* was determined by separation through HPLC and was detected fluorometrically (Shimadzu). Seawater samples (0.5−10 L) were filtered through combusted GF/F filters (Whatman). The filters were placed in 2 mL Nalgene vials, immediately shock-frozen in liquid nitrogen, and the vials stored at −80°C until extraction using 2 mL of 100% acetone for 24 hr at −20°C using 6 mL plastic scintillation vials. The extract was cleared by filtration through a 0.2 µm syringe filter (Spartan 13). Chl-*a* measurement in the extract was done using an HPLC system and the concentration (in µg L^{-1}) was calculated. For HPLC system calibration, pigment standards from DHI LAB products (Denmark) and Sigma-Aldrich (St. Louis, MO, USA) were used. The true concentrations of the standards were determined by spectrophotometric measurements using the specific extinction coefficient for each pigment based on Roy et al. (2011).

2.3.7. Bacterial and Viral Abundance via Flow Cytometry

Seawater samples (1.7 mL) were collected and glutaraldehyde (1% and 0.5% final concentration, respectively) added to fix bacterial cells and viruses. The samples were stored at −80°C after being flash-frozen in liquid nitrogen. Bacteria and viruses were counted after thawing using flow cytometry (FACSCalibur, Becton Dickinson, Oxford, UK) after Brussaard (2004) and Marie et al. (1999). For viruses, thawed samples were diluted in TE buffer (10 mM Tris HCl, 1 mM EDTA; pH 8). Bacteria and viruses were stained with SYBR Green I (molecular probes) and enumerated with a laser emitting at 488 nm and detected by their signature in a plot of side scatter (SSC) versus green fluorescence (FL1). Cell counts were determined with the CellQuest software (Becton Dickinson). Heterotrophic bacteria were distinguished from photosynthetic bacteria (*Prochlorococcus* spp. and *Synechococcus* spp.) by their signature in a plot of red fluorescence (FL2) versus green fluorescence (FL1). Yellow-green latex beads (1 µm, polysciences) were used as an internal standard (Gasol & Del Giorgio, 2000). Three distinct viral populations (V1–V3) were identified, the sum of the three populations is referred as "Virus."

2.4. Microbial Activities

Analyses of microbial metabolic activities are described in detail in Devresse et al. (2022). Briefly, PP was determined from ^{14}C incorporation according to Gargas (1975) and Nielsen (1952). Polycarbonate bottles (Nunc

EasYFlask, 75 cm^2) were filled with 260 mL prefiltered (mesh size of 200 µm) sample and spiked with 50 µL of a ~11 µCi $NaH^{14}CO_3^-$ solution (Perkin Elmer, Norway). Two-hundred microliters were removed immediately after spiking and transferred to a 5 mL scintillation vial for determination of added activity. Then 50 µL of 2N NaOH and 4 mL scintillation cocktail (Ultima Gold AB) were added. Duplicate samples from the top three depths at selected stations were incubated in 12 hr light and 12 hr dark at 22°C. Incubations were stopped by filtration of a 70 mL sub-sample onto 0.4 µm polycarbonate filters (Nuclepore). Particulate primary production (PP_{POC}) was determined from the material collected on the filter, while the filtrate was used to determine dissolved primary production (PP_{DOC}).

PP of organic carbon was calculated according to Gargas (1975):

$$\mathrm{PP}\left(\mu \mathrm{M\,C\,L^{-1}\,d^{-1}}\right) = \frac{a2 \times \mathrm{DI}^{12}C \times 1.05 \times k_1 \times k_2}{a1} \quad (2)$$

where $a1$ and $a2$ are the activities (DPM) (disintegrations per minute) of the added solution and the sample corrected for dark sample, respectively, and $DI^{12}C$ is the concentration (µM L^{-1}) of dissolved inorganic carbon (DIC) in the sample. DIC concentration was calculated from total alkalinity using the R package seacarb (Gattuso et al., 2020). The total alkalinity of the seawater was acquired through the open-cell titration method (Dickson et al., 2007). The value 1.05 is a correction factor for the discrimination between ^{12}C and ^{14}C, as the uptake of the ^{14}C isotope is 5% slower than the uptake of ^{12}C, k_1 is a correction factor for subsampling (bottle volume/filtered volume) and k_2 is the incubation time (d^{-1}). Total primary production (PP_{TOT}; µmol C L^{-1} d^{-1}) was derived from the sum of PP_{POC} and PP_{DOC} according to:

$$\mathrm{PP_{TOT}} = \mathrm{PP_{POC}} + \mathrm{PP_{DOC}} \quad (3)$$

Bacterial biomass production rates (BP) were measured through the incorporation of radiolabeled leucine (^3H) (specific activity 100 Ci $mmol^{-1}$, Biotrend) using the microcentrifuge method (Kirchman et al., 1985; Smith & Azam, 1992). Duplicate samples and one killed control (1.5 mL each) were labeled using ^3H-leucine at a final concentration of 20 nmol L^{-1}. All samples were incubated at 14°C in M156 and 13°C in M160 for 6 hr in the dark with headspace. Controls were poisoned with trichloroacetic acid. All Samples were measured on board with a liquid scintillation analyzer (Packard Tri-Carb, model 1900 A). ^3H-leucine uptake was converted to carbon units by applying a conversion factor of 1.55 kg C mol^{-1} leucine (Simon & Azam, 1989).

BP rates from incubations at 13°C and 14°C, respectively, were converted to BP rates at 22°C following the equation from López-Urrutia and Morán (2007):

$$\mathrm{BP_{22°C}} = \mathrm{BP_{14°C}} \times 1.906 \quad (4)$$

$$\mathrm{BP_{22°C}} = \mathrm{BP_{13°C}} \times 2.0716 \quad (5)$$

Community respiration rates (CR) were estimated from quadruplicate incubations by measuring changes of dissolved oxygen over 24−36 hr at the same temperature as used for BP (14°C in M156, 13°C in M160) using optode spot mini sensors (PreSens PSt3; Precision Sensing GmbH, Regensburg, Germany). The DL for CR was 0.55 µmol O_2 L^{-1} d^{-1}.

CR at 22°C was estimated using the extrapolation from Regaudie-De-Gioux and Duarte (2012):

$$\mathrm{CR_{22°C}(M156)} = \mathrm{CR_{14°C}} \times 2.011 - 0.013 \quad (6)$$

$$\mathrm{CR_{22°C}(M160)} = \mathrm{CR_{13°C}} \times 22,456 - 00,099 \quad (7)$$

2.4.1. Data Analysis

Statistical analyses and calculations were conducted using the software R (v4.0.2) in R studio (v1.1.414; Ihaka & Gentleman, 1996). Pearson correlation matrices were done with corrplot (Wei & Simko, 2021). Vertical and surface distribution figures were realized with R packages ggplot2 v3.3.3 (Wickham, 2016) using multi-level B-spline approximation (Lee et al., 1997) and inverse distance weighted interpolation (Kravchenko & Bullock, 1999), respectively.

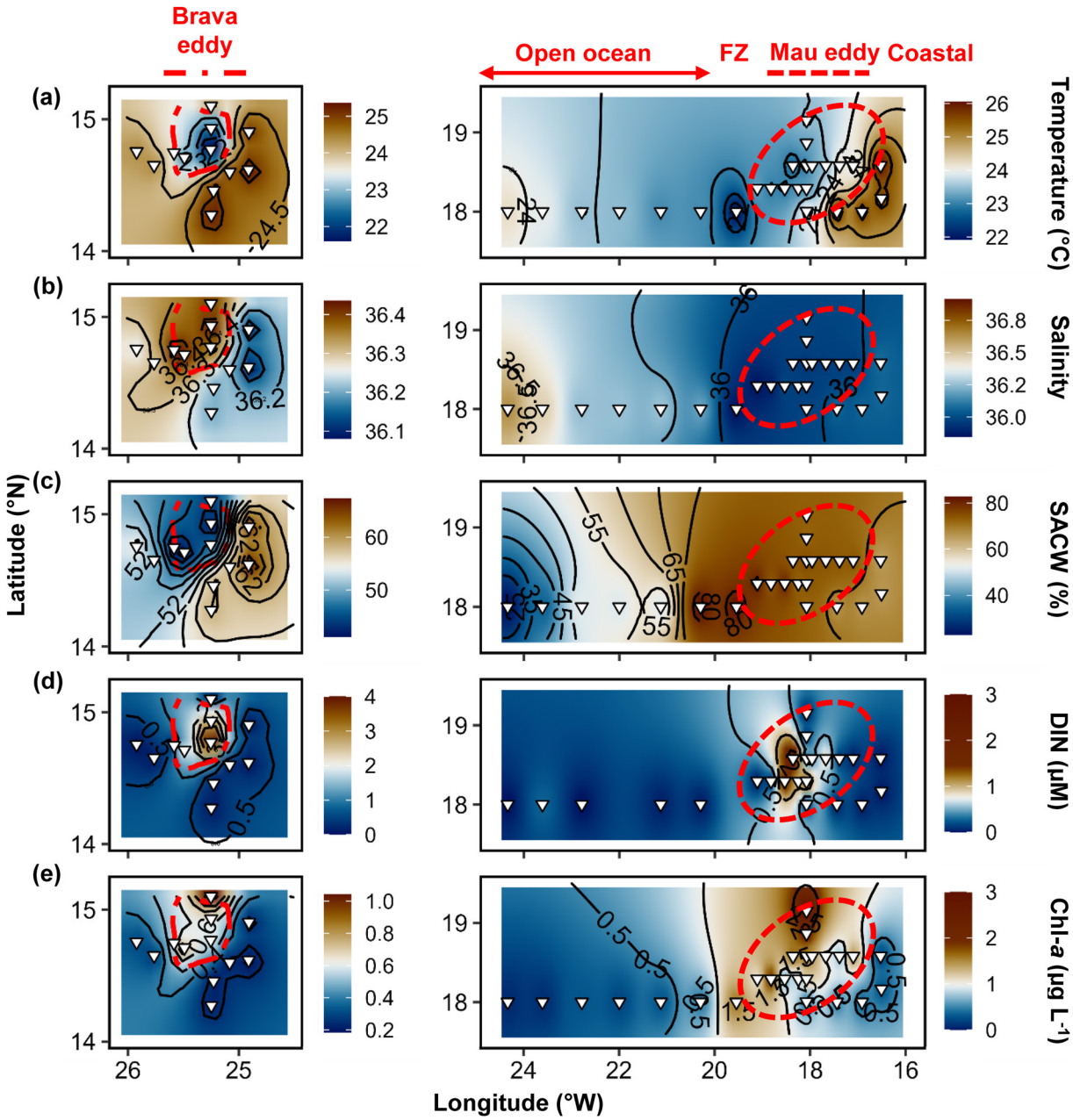

Figure 2. Surface (5−10 m depth) distribution of temperature (a), salinity (b), percentage of South Atlantic Central Water (SACW) (c), total inorganic nitrogen (DIN) (d), and Chl-*a* (e) in samples collected during cruises M156 (right) and M160 (left). Red dashed lines show the boundaries of the Mau and Brava eddies periphery. FZ refers to Frontal Zone.

3. Results

3.1. Hydrography

The regions of interest exhibit distinct differences in hydrography associated with local dynamics. Along the zonal transect, the open ocean waters (20°−24.5°W) had a surface (5−10 m depth) temperature range of 23.1°C–24.2°C and salinity between 36.19 and 36.63 (Figures 2a and 2b), whereas warmer (25.7°C−26.1°C) and fresher (36.06−36.08) water mass were found at the coastal stations (16.51°−16.92°W; Figures 2a and 2b). Within the Mau CE, the temperature ranges from 22.7°C to 24.2°C, while salinity of 35.84–35.99 were observed (Figures 2a and 2b). The Frontal Zone station E3 (19.55°W) temperature was 1°C colder than the adjacent stations (Figure 2a). The SACW contribution, calculated from temperature and salinity extrema, reveal the distribution and history

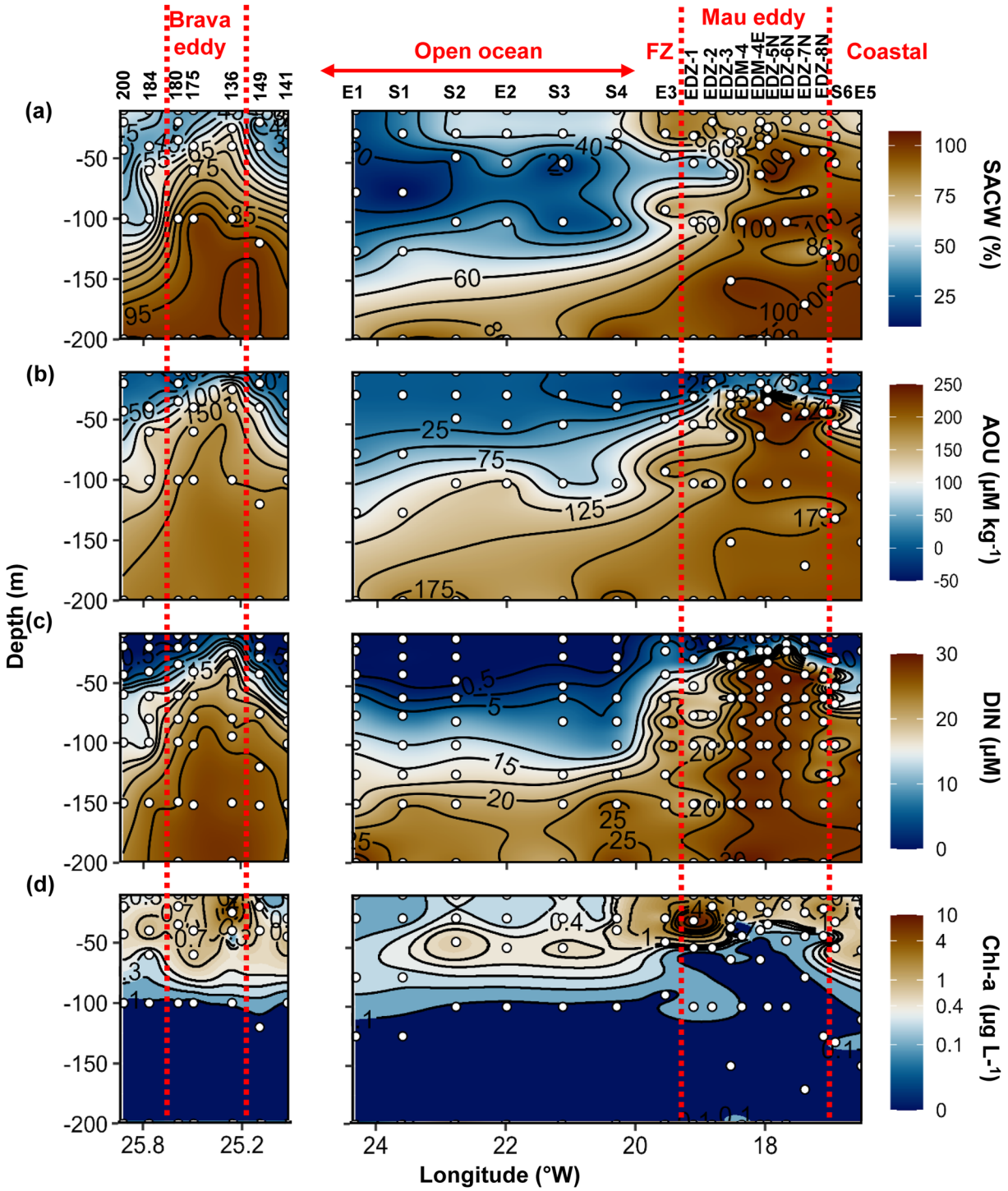

Figure 3. Vertical epipelagic distribution (0−200 m depth) of the percentage of South Atlantic Central Water (SACW) (a), apparent oxygen utilization (AOU) (b), total inorganic nitrogen (DIN) (c) and Chl-*a* (d) in samples collected during cruises M156 (right) and M160 (left). Red dashed lines show the boundaries of the Mau and Brava eddies' periphery. FZ refers to Frontal Zone.

of water masses. Surface distribution showed a decline in %SACW from the coast (65.0%−66.4%) toward the open ocean (22.9%−56.3%), albeit with higher values in the Mau eddy and at the frontal zone (71.6%−82.8%) (Figure 2c). At depth, SACW was evenly distributed within the epipelagic layer close to the coast (Figure 3a) with values >80%, except from the top 20 m where SACW was lower. In the Mau CE, the distribution of the SACW

across longitude (Figure 3a) was not evenly distributed with a half-circle curved form with SACW ranging between 40% and 70% in the inside between 30 and 100 m depth and >70% on the outside. In the open ocean, SACW was decreasing with depth and toward offshore, with SACW ~56% in the top 30 m depth at 20.3°W (St. S4) to 22.9% at 24.3°W (St. E1). The depth-distribution of AOU displays an increasing tendency toward the subsurface, but with a maximum within the Mau and Brava eddies (Figure 3b). In M160, surface temperature ranged between 20.9°C and 23.7°C with colder water mass in the core of the Brava CE (St.136), while salinity ranged between 36.39 and 36.44 (Figures 2a and 2b). The water mass comprised 40.6%−67.6% of SACW at the surface. The overall depth-distribution of SACW is quite similar to AOU, reaching ~62.9% at 25 m depth in the core (St. 136) of Brava CE, while averaging 43.9% ± 7% in the surrounding waters between 20 and 30 m depth (Figure 3a).

3.2. Biogeochemical Variability

In Mau and Brava eddies and at the frontal zone, elevated DIN (>1 μmol L^{-1}) concentrations were observed at the surface (Figure 2d). In those regimes, a compression of isopycnals with a strong doming of the nitraclines was observed (Figure 3c; Devresse et al., 2022). In contrast, DIN was depleted at the surface of both open ocean and coastal stations (<0.5 μmol L^{-1}; Figure 2d). This depletion in DIN extended down to ~40 m depth (Figure 3c) in the open ocean stations and to 5 m depth at the coastal ones. Deeper coastal waters (~80–200 m depth) were, on average, 3.4-fold richer in DIN than the open ocean waters.

Chl-*a* concentrations >0.5 μg L^{-1} were detected down to ~45−70 m depth in both eddies and at the Frontal Zone (Figure 3d). Higher values (>1 μg L^{-1}) were observed in and near the core of the Brava eddy (St.136 at 25 m depth, Figure 3d; St. 134 at 68 m depth; data not shown) and all across the Mau eddy (Devresse et al., 2022). Chl-*a* was low at the surface of the open ocean (<0.5 μg L^{-1}) compared to values between 0.20 and 1.47 μg L^{-1} at the coastal stations (Figure 2e). Chl-*a* maxima in the open ocean were located around ~75 m from 23.61° to 24.33°W and around ~50 m from 22.78° to 20.3°W, with concentrations up to 0.68 μg L^{-1} (Figure 3d). At the coastal stations, the Chl-*a* maxima were found between 30 and 40 m with values up to 0.96 μg L^{-1}.

We observed a relative depletion in surface DOC at the center of both Mau and Brava eddies, with values of 78 μmol L^{-1} (St. EDZ−5°N) and 59 μmol L^{-1} (St. 136), respectively. DOC concentrations at the surface (Figure 4a), ranged from 57.5 to 108 μmol L^{-1}, with higher values in all stations collected during M156 than in those collected during M160. DOC distributions (Figure 5a) showed a compression of isopycnals with a dome shape in both eddies, but contrarily to DIN, waters uplifted had lower DOC concentrations.

Semi-labile DOC (SL-DOC) concentration (Figures 4b and 5b) and its fraction of the DOC (Figures 4c and 5c) varied considerably during M156 ranging from 1.4 to 54.4 μmol L^{-1}, representing 2.3 to 70.8% DOC. In contrast, during M160, SL-DOC variations were lower with SL-DOC ranging between 0.7 and 6.8 μmol L^{-1} representing 1.5 to 11.7% DOC. Below 50 m depth, SL-DOC >5% DOC was found sporadically in samples collected during the cruise M156, whereas it was found only in the Brava eddy during the cruise M160 (except St.168, 60 m depth; data not shown; Figures 4c and 5c).

DON concentration ranged between 2.2 and 10.2 μmol L^{-1} at the surface and its distribution showed opposite trends between the Mau and Brava eddies (Figure 4d). DON concentration was more elevated within the Mau eddy (>8 μmol L^{-1}) and more depleted within the center of the Brava eddy (St.136; 2.2 μmol L^{-1}) compared to their respective surrounding waters. DON distribution (Figure 5d) was contrasted during cruise M156, with elevated values (>5 μmol L^{-1}) between 50 and 200 m depth from the eddy center (St. EDM-4) to open ocean St. S1. During cruise M160, depth distribution did not show the contrasting difference between eddy and non-eddy stations.

Semi-labile DON (SL-DON) concentration varied from 0.15 to 3.49 μmol L^{-1} (Figures 4e and 5e) representing 3–42.6%DON (Figure 4f and Figure S3a in Supporting Information S1). SL-DON and its fraction of the DON at the surface were more elevated in the Mau eddy whereas in the Brava eddy, SL-DON was slightly depleted but its fraction of the DON was higher compared to their surrounding waters (Figures 4e and 4f). SL-DON concentration decreased with depth in both cruises. In samples collected during M160, the semi-labile DON concentration was lower than in the samples collected during M156, while their fraction of the DON was higher representing on average 9.5 ± 5.7%DON in M156 and 14.4 ± 7.6%DON in M160 (Figure S3a in Supporting Information S1).

3.3. Microbial Metabolic Activities

Microbial metabolic activities (BP, CR, PP_{DOC}, PP_{TOT}) distribution were extensively described for the cruise M156 in Devresse et al. (2022). Briefly, microbial metabolic activities were all enhanced within the Mau eddy

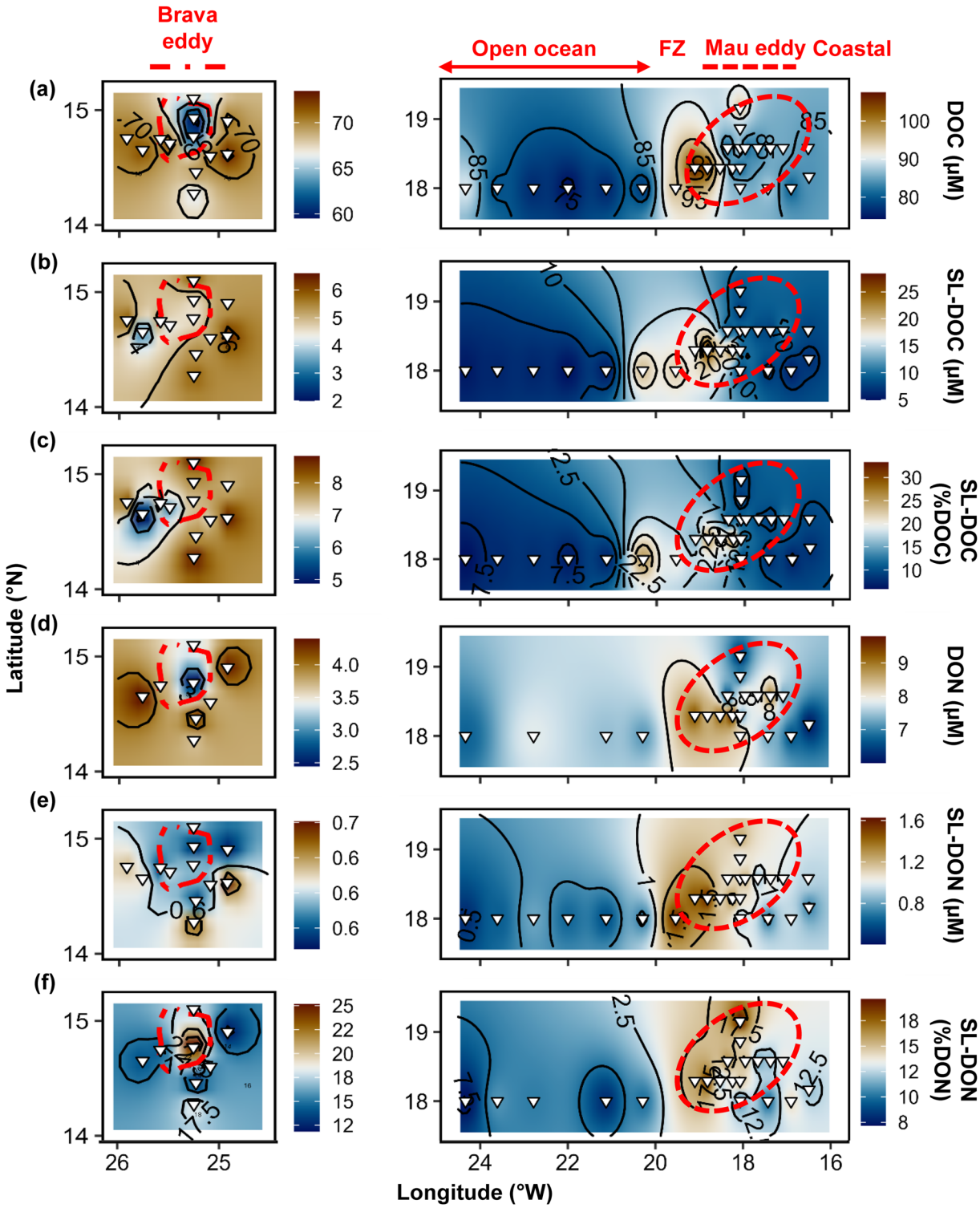

Figure 4. Surface (5−10 m depth) distribution of dissolved organic carbon (DOC) (a), semi-labile DOC (SL-DOC) (b), semi-labile DOC as % of DOC (c), dissolved organic nitrogen (DON) (d), semi-labile DON (SL-DON) (e), and semi-labile DON as % of DON (f) in samples collected during cruises M156 (right) and M160 (left). Red dashed lines show the boundaries of the Mau and Brava eddies periphery. FZ refers to Frontal Zone.

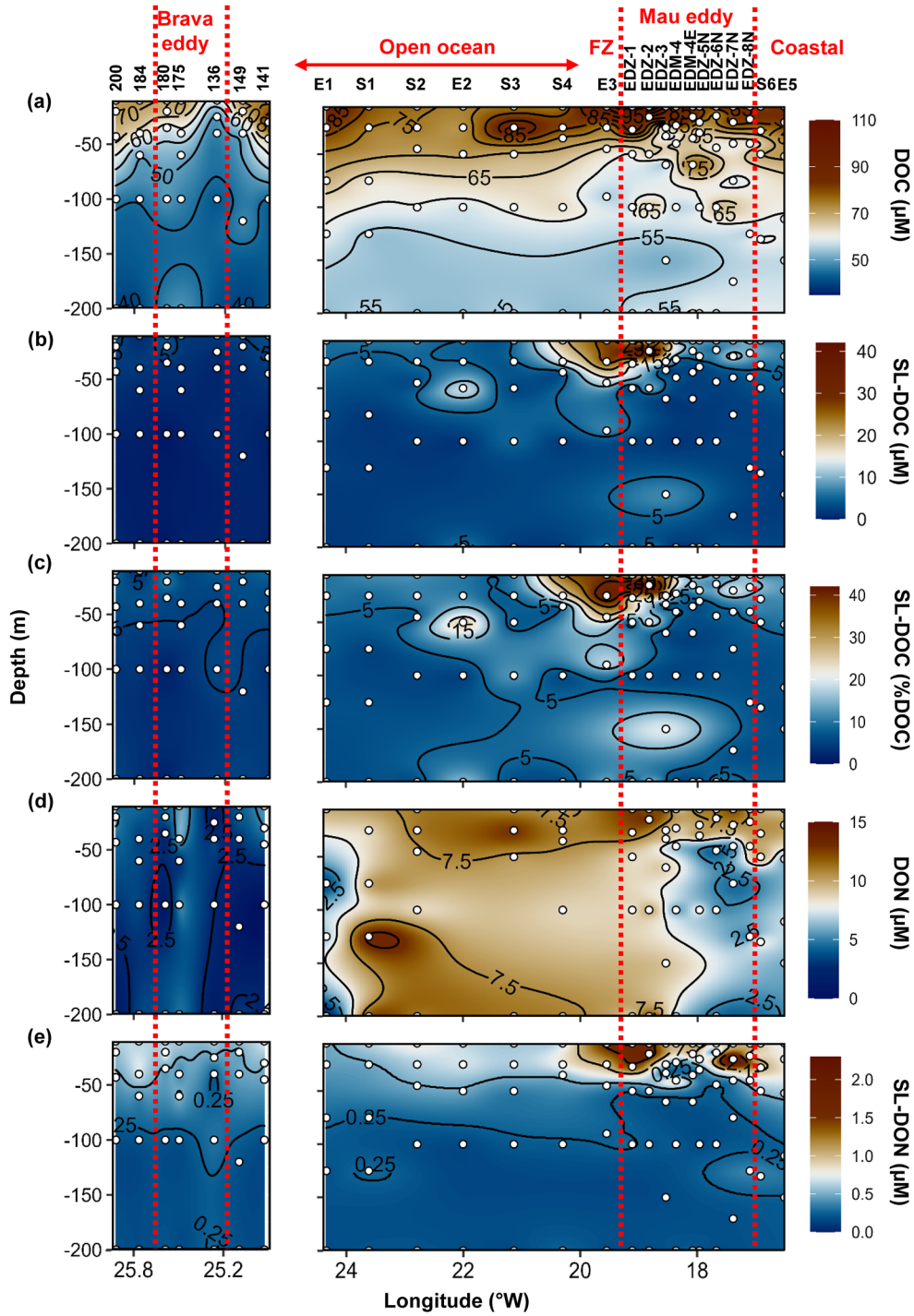

Figure 5. Vertical epipelagic distribution (0–200 m depth) of dissolved organic carbon (DOC) (a), semi-labile DOC (SL-DOC) (b), semi-labile DOC as % of DOC (c), dissolved organic nitrogen (DON) (d), and semi-labile DON (SL-DON) (e) in samples collected during cruises M156 (right) and M160 (left). Red dashed lines show the boundaries of the Mau and Brava eddies' periphery. FZ refers to Frontal Zone.

compared to the open ocean and coastal waters, although with spatial strong variability. During M160, the sampling coverage did not allow to evaluate the spatial variability of microbial metabolic activities across the Brava eddy. Yet, an increase of all microbial metabolic activities was observed in Brava eddy stations compared to those outside the eddy (Figure 6).

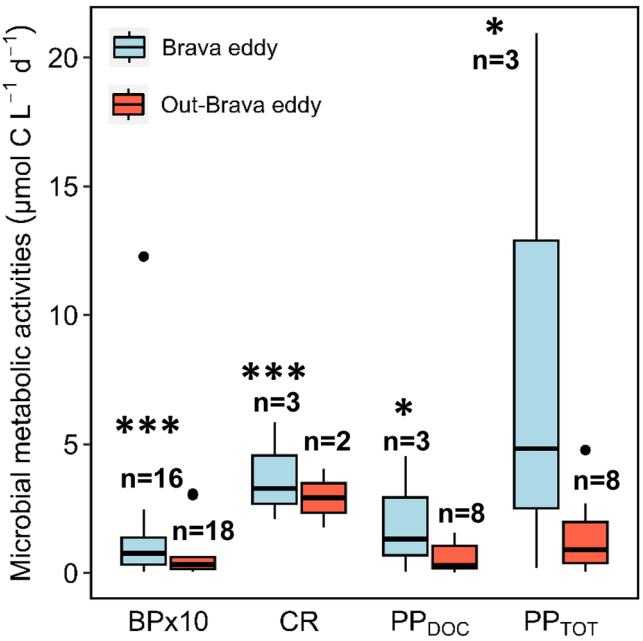

Figure 6. Epipelagic distribution (≤100 m depth) of bacterial production (BP), community respiration (CR), dissolved primary production (PP_{DOC}), and total primary production (PP_{TOT}) within Brava eddy and outside Brava eddy stations during cruise M160. Note that BP rates have been multiplied by 10. *t* test statistical significance: "***"<0.001, "**"<0.01, "*"<0.05. *n* is the sample size.

3.4. PARAFAC Analysis and Optical DOM Distribution

PARAFAC analysis of our complete FDOM EEM data set decomposed four independent components, two humic-like (C468 and C398) and two protein-like (C340 and C306) closely related to Coble peaks (Coble, 1996). The calculated excitation and emission spectra for each of the four components are shown in Figure S2 in Supporting Information S1. Component C468 had elements that were similar to classical terrestrial humic-like components (A and C-peaks), Ex/Em: 230-365/468. Component C398 was similar to a marine humic-like component (M peak), Ex/Em: 230-315/398. Component C340, and Component C306, were similar to the tryptophan-like T-peak and tyrosine B-peak with Ex/Em: 230-275/340 and 230-265/306, respectively.

3.4.1. Optical DOM Distribution During M156

In the surface samples collected during M156, fluorescence intensities of components C468 and C398 decreased from the coast to the open ocean with values decreasing from 0.024 to 0.012 RU for C468 and from 0.019 to 0.007 RU for C398 (Figures 7a and 7b). The Mau eddy and the frontal zone (17.10°–19.55°W) showed a clear contrast, with fluorescence intensities of 0.025–0.047 and 0.017−0.029 RU for C468 and C398, respectively. Depth distribution of fluorescent components in the epipelagic layer (0−200 m depth) were clearly different whether samples were collected in eddy-influenced stations (Mau, FZ, Brava), in coastal stations or in open ocean stations (Figure 8). At the coastal stations, fluorescence intensities of C468 and C398 were lower in the top ∼20 m depth, reached their maximum in the subsurface between ∼30 and 50 m depth, and stayed rather constant between ∼50 and 200 m depth (Figures 8a and 8b). In contrast, fluorescence intensity of C468 was rather constant in the epipelagic layer in the open ocean stations apart from the furthest offshore station (23.6°–24.3°W; St. E1 and S1), where C468 was depleted within the top 25 m (Figure 8a). Fluorescence intensity of C398 in the open ocean was decreasing with depth and was decreasing toward offshore with values >0.023 RU present from 5 m depth at 20.3°W (St. S4) and present from 75 m depth at 24.3°W (St. E1; Figure 8b). In the Mau eddy and at the frontal zone, fluorescence intensities of both components were decreasing with depth, with values >0.025 RU reaching down to 75 m depth in the Mau CE and down to 45 m depth at the frontal zone (Figures 8a and 8b). Below ∼50−75 m depth, fluorescence intensities of C468 and C398 were rather constant in the Mau CE and the frontal zone.

At the surface, fluorescence intensity of component C340 decreased from the coast to the open ocean, with values decreasing from 0.042 to 0.013 RU (Figure 7c). In contrast, elevated C340 fluorescence was found at the surface of the Mau eddy and the frontal zone ranging between 0.037 and 0.10 RU, respectively (Figure 7c). That pattern was also visible in the upper 30−40 m depth (Figure 8c) with C340 fluorescence intensity >0.05 RU within the eddy. In the epipelagic layer of both cruises, the fluorescence intensity of C340 decreased with depth.

Fluorescence intensity of component C306 at the surface increased from the coast to the open ocean, with fluorescent intensity ranging between 0.017 and 0.024 RU (Figure 7d). In opposition, fluorescence intensity of C306 was lower at the surface of the Mau eddy and the frontal zone ranging between 0.009 and 0.019 RU (Figure 7d). In the epipelagic layer, fluorescence intensity of C306 was lower in the coastal, Mau eddy and in the frontal zone stations with values <0.025 RU (apart from St.EDZ-7N at 75 m) which is in contrast to the open ocean stations where values were >0.03 RU in the top ∼50−100 m depth (Figure 8d).

In the surface samples, $a_{CDOM}(325)$ was decreasing from the coast to open ocean during M156 with values ranging from 0.72 to 0.26 m^{-1} (Figure 7e). In contrast, elevated $a_{CDOM}(325)$ values were found in the Mau eddy and the frontal zone, ranging between 0.46 and 1.18 m^{-1} (Figure 8e). Depth-distribution showed that $a_{CDOM}(325)$ remained fairly constant in the epipelagic layer from the coast to the open ocean with maximum values at ∼50 m depth. In the Mau eddy and the frontal zone, depth distribution was not uniform with $a_{CDOM}(325)$ concentration >0.4 m^{-1} reaching down to ∼100 m depth at the Frontal Zone and the western part of the eddy and down to ∼40 m depth in the eastern part of the eddy (Figure 8e).

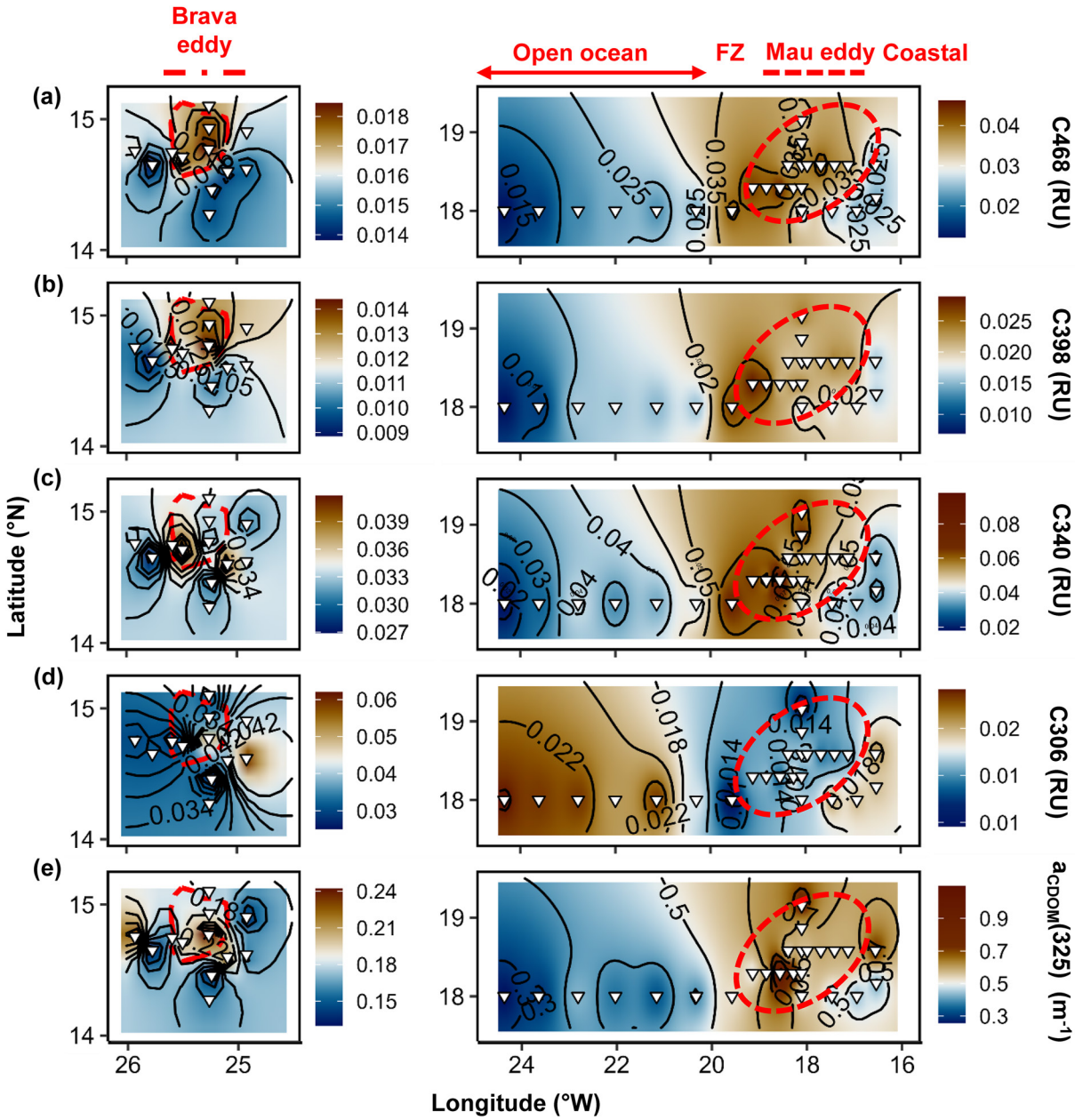

Figure 7. Surface (5−10 m depth) distribution of fluorescent components C468 (a), C398 (b), C340 (c), C306 (d), and $a_{CDOM}(325)$ (e) in samples collected during cruise M156 (right) and M160 (left). Red dashed lines show the boundaries of the Mau and Brava eddies' periphery. FZ refers to Frontal Zone.

3.4.2. Optical DOM Distribution During M160

In the surface samples collected during M160, fluorescence intensities of components C468 and C398 ranged between 0.013 and 0.019 RU and 0.008−0.015 RU, respectively, at the surface (Figures 7a and 7b), lower than those found in the Mau eddy. The highest fluorescence intensities for C468 and C398 were found in the Brava CE, especially in the core (St. 136). Depth distribution of fluorescent components in the epipelagic layer (0−200 m depth) were clearly different whether samples were collected in eddy-influenced stations (Mau, FZ, Brava), in coastal stations or in open ocean stations (Figure 8). In the Brava eddy, C468 and C398 depth distribution revealed compression of isopycnals with a dome shape toward the surface of the CE core (St.136; Figures 8a and 8b).

No clear spatial differences in fluorescence intensity of component C340, between the Brava CE and its surrounding waters were observed at the surface with C340 fluorescence intensity ranging between 0.026 and 0.044 and

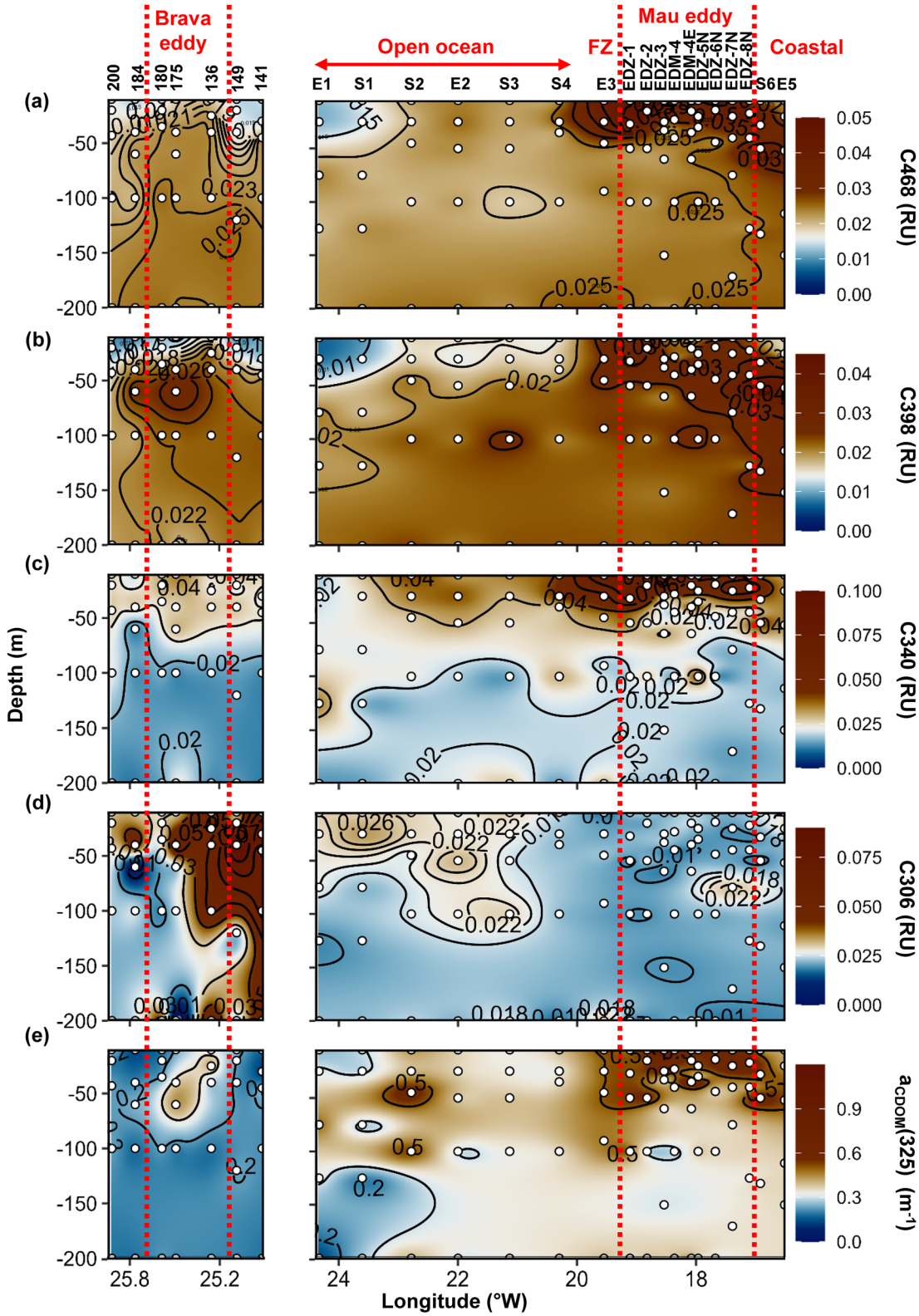

Figure 8. Epipelagic distribution (0−200 m) of fluorescent components C468 (a), C398 (b), C340 (c), C306 (d), and $a_{CDOM}(325)$ (e) in samples collected during cruises M156 (right) and M160 (left). Red dashed lines show the boundaries of the Mau and Brava eddies' periphery. FZ refers to Frontal Zone.

0.028−0.042 RU, respectively. Depth distribution of C340 fluorescence intensity showed no clear differences between stations within Brava eddy and those outsides (Figure 8c).

Fluorescence intensity of components C306 at the surface (Figure 7d) was higher than in samples collected during M156 but it showed no clear spatial differences between the Brava CE and its surrounding waters with values ranging between 0.028 and 0.054 and 0.025−0.062 RU, respectively. Fluorescence intensity of C306 showed high values (>0.04 RU) vertically distributed from the surface to 200 m depth in three stations (St.134, 136, and 141), whereas in other stations, C306 was decreasing with depth with maximum values at ∼50 m depth (Figure 8d).

During M160, the $a_{CDOM}(325)$ range at the surface (0.12–0.26 m^{-1}) was lower with slightly higher values in the center of the Brava eddy (Figure 7e). Depth-distribution showed that $a_{CDOM}(325)$ was higher in the top ∼50 m depth of the Brava CE compared to the surrounding waters (Figure 8e).

3.5. Relationships Between Physical and Biogeochemical Parameters and Fluorescent Components

We applied a Pearson correlation matrix (Figure 9) to reveal correlations between CDOM and FDOM components with the measured parameters for both cruises. Humic-like components C468 and C398 were significantly correlated ($p < 0.001$) to physical (temperature, oxygen, AOU) and biogeochemical (DOC) parameters and to inorganic nutrient (DIN) in samples collected during M160 whereas, in samples collected during M156, those relationships were weaker. Direct representation by scatter plots showed that those relationships diverged especially in the Mau eddy and coastal stations (Figure S4 in Supporting Information S1). During M156, C468 showed the most significant correlations ($p < 0.001$) with microbial metabolic activities (PP_{DOC}, PP_{TOT}, BP, CR), SL-DON, phytoplankton (Chl-*a*) and viruses abundance (Figure 9 and Figure S4 in Supporting Information S1).

In both cruises, tryptophan-like component C340 was significantly correlated ($p < 0.001$) to microbial metabolic activities (BP, CR) and semi-labile dissolved organic matter (SL-DON, SL-DOC) and phytoplankton biomass (Chl-*a*; Figure 9 and Figure S4 in Supporting Information S1). Tyrosine-like component C306 was significantly correlated ($p < 0.001$) to physical parameters (temperature, salinity, oxygen) in M156, albeit weakly and was not correlated to any variable ($p > 0.05$) in M160 (Figure 9). $a_{CDOM}(325)$ was significantly correlated ($p < 0.001$) to Chl-*a*, PP_{DOC}, PP_{TOT}, and bacterial production for both cruises albeit a stronger correlation (r) for samples collected during M160 than for samples collected during M156 ($r = 0.94, 0.63, 0.69, 0.87$ and $r = 0.34, 0.40, 0.39, 0.39$, respectively; Figure 9).

4. Discussion

4.1. FDOM Components

We identified four FDOM components (Figure S2 in Supporting Information S1) that were related to the traditional A and C (C468), M (C398), T (C340), and B (C306) peaks (Coble, 1996). Fluorescent component C468 is commonly referred to as a "terrestrial" humic-like component and C398 as a marine humic component. However, both are ubiquitous in marine environments (Catalá et al., 2015; Jørgensen et al., 2011; Kowalczuk et al., 2013) as peaks similar to peak C were also found to be produced by different phytoplankton and bacterial groups (Chari et al., 2013; Fukuzaki et al., 2014; Romera-Castillo et al., 2010, 2011). Both components are produced through microbial reworking of labile DOM, and directly by phytoplankton (Arai et al., 2018; Coble, 1996; Romera-Castillo et al., 2010, 2011; Shimotori et al., 2009). In our study, C468 and C398 correlated significantly with AOU in the cruise M160 and with community respiration in both cruises. This is consistent with published studies were both components were correlated to AOU (Hayase & Shinozuka, 1995; Martínez-Pérez et al., 2019; Tanaka et al., 2014; Yamashita et al., 2007) and to bacterial respiration (Omori et al., 2020). Therefore, C468 and C398 are suitable tracers of DOM mineralization as by-product of microbial respiration.

C340 is a tryptophan-like component produced by both phytoplankton and heterotrophic bacteria (Coble, 1996; Ortega-Retuerta et al., 2021; Romera-Castillo et al., 2010; Shimotori et al., 2009, 2012). Our correlation analyses confirm that C340 is a good indicator of semi-labile DON measured here, in accordance with previous studies (Lønborg et al., 2015) and that C340 might also indicate dissolved amino acid abundance (Yamashita & Tanoue, 2003). The correlation of C340 with microbial activities indicates that C340 was produced in situ by phytoplankton within the eddies, thanks to nutrients made available by upwelling. Our results coincide with a previous study where tryptophan-like FDOM was positively correlated to leucine-aminopeptidase activity,

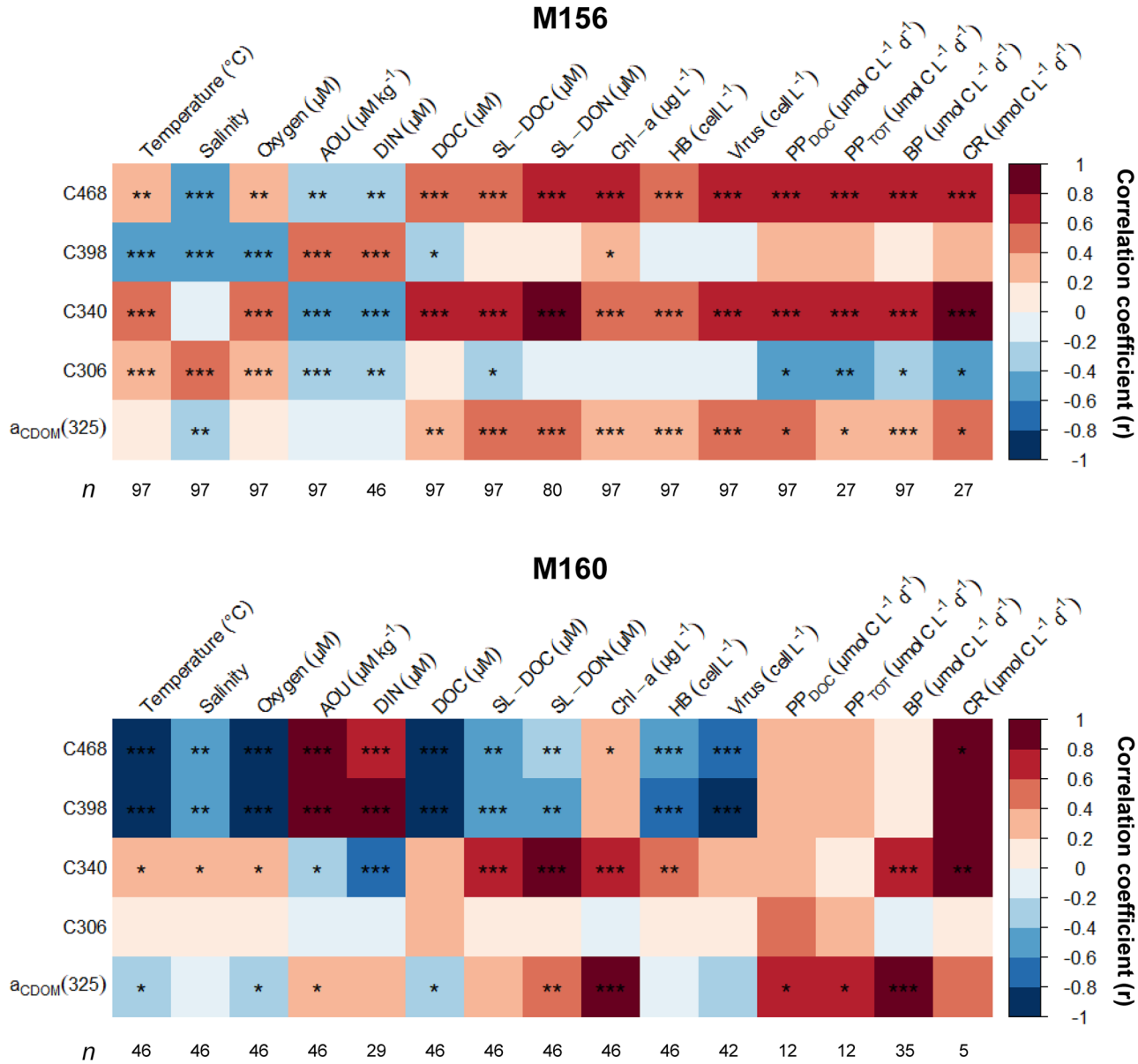

Figure 9. Pearson correlation matrix of fluorescent dissolved organic matter components and $a_{CDOM}(325)$ against various biochemical variables and microbial activities in the upper 100 m depth from samples collected during M156 and M160. Statistical significance: "***"<0.001, "**"<0.01, "*"<0.05. *n* is the sample size used in Pearson correlations.

bacterial production, and recently produced HMW-DOM (Fox et al., 2017; Hudson et al., 2008; Maie et al., 2007; Teira et al., 2012; Williams et al., 2010).

C306 emitted fluorescence in the same Ex/Em as the tyrosine-like components or peak B (275/310 nm). However, it did not correlate with tyrosine concentration (data not shown), and only poorly to all other parameters investigated in this study. Protein-like fluorescence occurs in a wavelength region that is easily contaminated by a variety of sources including marine paints or epoxies (Murphy et al., 2004). CDOM/FDOM samples were collected in the ship wet lab where air could circulate easily. During M160, FDOM component C306 was likely contaminated by painting aerosols as blanks realized with the same procedure as the samples showed high fluorescence for C306 (0.026–0.052 RU; $n = 23$) but not for the other FDOM components (<0.01 RU; average 0.003 ± 0.003 RU; $n = 23$).

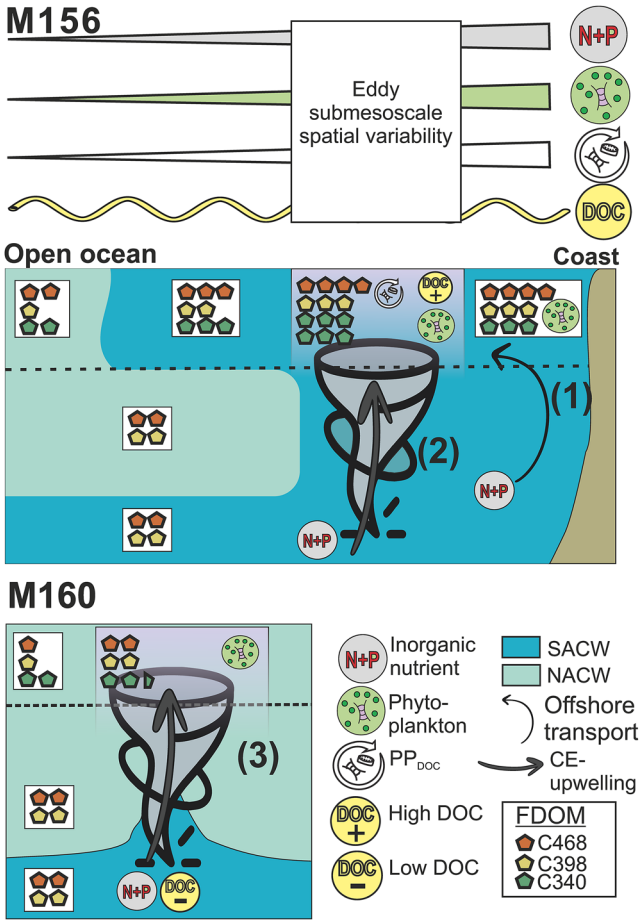

Figure 10. Schematic model of processes influencing the distribution of fluorescent dissolved organic matter (FDOM) components in cruises M156 and M160. (a) During cruise M156, offshore transport of South Atlantic Central Water (SACW) water generated a gradient along the coast to the open ocean of inorganic nutrients, phytoplankton biomass, extracellular release rate of carbon (PP_{DOC}), humic-like FDOM components (C468 and C398) while dissolved organic carbon (DOC) concentration fluctuated and protein-like FDOM C340 remained rather constant. (b) The Mau eddy incorporated coastal-SACW rich in humic-like FDOM during his formation. The upwelling within the Mau eddy generated variability at submesoscale of phytoplankton biomass, PP_{DOC} and DOC. On average, PP_{DOC} rates and DOC concentrations were higher than in coastal and open ocean waters. Thus within the Mau eddy, fluorescence intensities of protein-like FDOM component C340 and of humic-like FDOM components C468 and C398 were higher due to increase of primary productivity and DOM remineralization respectively. (c) During cruise M160, the Brava eddy was out of coastal-dynamic influence. Water upwelled within the eddy had higher SACW%, higher fluorescence of humic-like FDOM components C468 and C398 and lower DOC concentration. The upwelling of nutrients associated with the Brava eddy generated slightly higher phytoplankton biomass, PP_{DOC}, and protein-like FDOM component C340 than in surrounding waters.

4.2. Factors Controlling the Distribution of Fluorescent Dissolved Organic Matter in the CEs

The two CEs (Mau and Brava eddies) showed similarities by (a) inducing more phytoplankton biomass (Chl-*a*) due to nutrient upwelling and (b) containing more humic- and protein-like FDOM within them consistently with previous studies (Chiranjeevulu et al., 2014; Wang et al., 2017; M. Zhang et al., 2020; Y. Zhang et al., 2009). Yet, the CEs showed disparities in the distribution of FDOM components, especially humic-like FDOM. During the cruise M160, humic-like FDOM components C468 and C398 correlated significantly with DIN, and physical (temperature, oxygen) and biogeochemical (DOC) parameters highlighting well the upwelling occurring in the CE. In contrast, those correlations were weaker (for C398) and even inverse (for C468) during cruise M156 and the humic-like FDOM components distribution did not follow the upwelling (Figure 2 and Figure S4 in Supporting Information S1; Devresse et al., 2022). We propose two hypotheses regarding those differences that are depicted in Figure 10:

1. The Mau eddy trapped coastal water enriched in humic-like FDOM during his formation. Surface waters of the Mauritanian coast has been shown to be enriched in humic-like FDOM (similar to C468 and C398) during the upwelling season (December–April) (Heller et al., 2016). The upwelling season is also characterized by the advection of deep SACW (Barton et al., 1998; Mittelstaedt, 1983, 1991). In the ETNA, coastal-eddy generation reaches its maximum during the relaxation season (May–July) (Schütte et al., 2016). During this season, the coastal water mass is characterized by high %SACW (>80%; Klenz et al., 2018), which was also observed during cruise M156. Coastal eddies incorporate SACW-rich coastal waters during their formation (Dilmahamod et al., 2022; Schutte et al., 2016) and thus might incorporate humic-like FDOM-rich waters. In contrast, the Brava eddy was sampled in the vicinity of Brava Island, a hotspot of wind-formed eddies far from the influence of coastal dynamic (Cardoso et al., 2020; Chavanne et al., 2002; Schütte et al., 2016). Therefore, the upwelling was also visible from the distribution of %SACW and humic-like FDOM components C468 and C398.
2. The Mau eddy had higher production rates of humic-like FDOM compared to the Brava eddy. The Mau eddy was more productive than the Brava eddy, elevated phytoplankton biomass (Chl-*a* >1 μg L^{-1}) were widespread across the Mau eddy whereas only close to the core in the Brava eddy (Figure 3; Devresse et al., 2022). Thus more semi-labile DOM materials (SL-DOC, SL-DON, C340) were produced and recycled within the Mau eddy leading to higher production rates of humic-like FDOM as by-product of microbial respiration. Catalá et al. (2015) showed for the dark ocean that a component close to C468 had a production rates 19-fold higher than a component close to C398 which might explain why CR was correlated to C468 and not to C398 during M156 (Figures 9 and 10). Moreover, humic-like FDOM production through a biological reworking of labile DOM is enhanced when humic precursors are already present (Aparicio et al., 2015). Therefore, inside the Mau eddy, freshly produced DOM due to upwelled waters, mixed with old/persistent humic DOM might have enhanced humic-like FDOM production rates. This might explain why C468 was positively correlated to SL-DOM and bacterial production during cruise M156 and not during cruise M160.

4.3. Additional Factors Controlling the Distribution of Fluorescent Dissolved Organic Matter in the ETNA

Yet, a question remains about why the fluorescence intensities of humic-like FDOM (C468 and C398) were relatively high in the near-surface waters during cruise M156 compared to cruise M160. During the relaxation season, coastal waters are transported offshore through currents and eddies (Pelegrí & Peña-Izquierdo, 2015; Schütte et al., 2016). This was characterized by the decreasing %SACW toward offshore in the cruise M156. SACW is nutrient-rich compared to NACW (Pelegrí & Peña-Izquierdo, 2015). Thus, a progressive decline in primary productivity and phytoplankton biomass was observed from the coast to the open ocean (Devresse et al., 2022). Loginova et al. (2015) found that the component C468 is produced from DOM by bacteria proportionally to DIN supply. Therefore, the offshore export of nutrient-rich SACW must have enhanced the microbial degradation of DOM with the production of the component C468 along the 900 km transect.

Moreover, we did not observe a clear gradient of DOC and SL-DOC between coastal and open ocean stations. This is consistent with Valiente et al. (2022), who reported DOC values in the same area during June 2017 with relatively high values (>80 μmol L^{-1}) interspersed with areas of low concentration. DOC relative accumulation can be explained by inorganic nutrient availability limiting its microbial degradation (e.g., Alonso-Sáez et al., 2007) and by a turnover time of weeks to months of the semi-labile DOC (Hansell et al., 2009).

Other factors, such as viral infection likely co-occurred. Marine virus particles-like abundances range between 10^6–10^{11} L^{-1} (see review by Parikka et al., 2017), and we report here elevated values (2×10^9–1.75×10^{11} L^{-1}) in samples collected during M156 (Figures S3b and S4 in Supporting Information S1). Viral abundance significantly correlated with C468 and C340 (Figure 9 and Figure S4 in Supporting Information S1). Therefore, we suspect that viruses through their lytic activities were an important driver of humic and protein-like FDOM. The effects of viruses on FDOM are still poorly understood. However, Lønborg et al. (2013) and X. Xiao et al. (2021) found that viral lysis led to an increase of both humic and protein-like components in the cultures of *Micromonas pusilla* and in the cyanobacteria *Prochlorococcus,* which is coherent with our observations during cruise M156.

CDOM absorption at 325 nm is due to aromatic compounds (Coble, 1996; Jørgensen et al., 2011). The similar distribution of $a_{CDOM}(325)$ with C398 and C468 during cruise M156 suggests that it is a tracer for the production of the aromatic humic-like DOM during the microbial degradation of labile and semi-labile DOM (Catalá et al., 2016; Coble, 1996; Jørgensen et al., 2014). Nelson and Siegel (2013) reported $a_{CDOM}(325)$ to vary from 0.005 to 0.25 m^{-1} in open ocean waters. Here, we report relatively high values in the cruise M156 (>0.3 m^{-1} all along the 900 km transect), which suggests, in accordance with Lovecchio et al. (2018); that in the Mauritanian upwelling system, organic carbon can be transported offshore.

Similar components to C468 and C398 reported by Catalá et al. (2015) have a long turnover time in the dark ocean (C1 an C2 with 435 ± 41 and 610 ± 55 years, respectively in Catalá et al., 2015), whereas in euphotic zone their removal occurs within days due to photodegradation (Helms et al., 2013; Miranda et al., 2020; Timko et al., 2015; Zhu et al., 2017). Therefore, they are typically depleted at the surface of subtropical marine waters (Jørgensen et al., 2011; Yamashita et al., 2017). The fact that the humic-like FDOM signature remained high at the surface until 700 km offshore during cruise M156 is thus surprising. Satellite-based aerosol measurements showed more aerosol during M156 than during M160 (TOMS AI; Figure S4 in Supporting Information S1). Those aerosols were likely related to Saharan dust as its export through the ETNA reaches a maximum in July and a minimum in November–December (Engelstaedter & Washington, 2007). Therefore, Saharan dust might have attenuated UV exposure during cruise M156, limiting the photodegradation of humic-like FDOM (Herman et al., 1999; Smyth, 2011). Moreover, Saharan dust can also be a source of humic-like FDOM, especially of FDOM peak M (C398) (Campanero et al., 2022; Sánchez-Pérez et al., 2016) and iron contained in dust and associated with humic substances might also attenuate photodegradation in surface waters (Y. H. Xiao et al., 2013).

Overall, our results showed that microbial processes increased the humic-like FDOM content of the waters during the cruise M156. Therefore, in areas where offshore transport of organic matter coexists with intense sub-mesoscale processes (eddies, filament, meander), component C468 is not suitable for tracking upwelling in CEs. However, component C468 may be useful to track upwelling as a complementary index in oligotrophic areas such as the Atlantic gyres, where metabolic activities are relatively low (Serret et al., 2015). Component C398 was related to temperature and DIN in both eddies. Our results suggest a lower production rates of component C398 compared to component C468, in accordance with Catalá et al. (2015) (C2 and C1 in their study). Thus

C398 is less impacted by microbial metabolic activities and appears to be a suitable marker to track upwelling in CEs.

5. Conclusion

- Our study highlights that humic-like FDOM, mostly C398, enable tracing nutrient upwelling by eddies, while protein-like FDOM and $a_{CDOM}(325)$ are good indicators of the high activity (e.g., bacterial production) associated with these eddies. However, in coastal areas, tracing nutrient with humic-like FDOM can be challenging as eddies might incorporate humic-like FDOM rich water during their formation, masking the upwelling signal. Continuous FDOM data obtained with sensors attached to gliders, floats, or the CTD-rosette could help to better follow eddy development and influence. Most FDOM sensors indeed record at Ex/Em of 370/450 nm; near the intensity maximum of our C468 component. We recommend that further eddies studies should be complemented using such tools.

Data Availability Statement

All data are available at the PANGEA database https://doi.pangaea.de/10.1594/PANGAEA.959742 and https://doi.org/10.1594/PANGAEA.950510.

Acknowledgments
We thank the captain and the crew of the *R/V Meteor* for their support during the cruises M156 and M160. We thank J. Roa, T. Klüver, L. Scheidemann, S. Golde, and H. Hepach for sampling on board. We thank J. Roa and S. Golde additionally for the analysis of dissolved organic matter and T. Klüver for cell counting, bacterial and phytoplankton activities analyses. We thank B. Domeyer, R. Suhrberg, and B. Bogner for the nutrient analyses. We thank K. Heymann, M. Hieronymi, and R. Röttgers for providing the Chlorophyll-*a* data for cruise M160. We are very thankful to two anonymous reviewers for their valuable comments. This study is a contribution of the REEBUS project (Role of Eddies in the Carbon Pump of Eastern Boundary Upwelling Systems) sub-projects WP1 and WP4, funded by the BMBF (funding reference no. 03F0815A). Open Access funding enabled and organized by Projekt DEAL.

References

Alonso-Sáez, L., Gasol, J. M., Arístegui, J., Vilas, J. C., Vaqué, D., Duarte, C. M., & Agustí, S. (2007). Large-scale variability in surface bacterial carbon demand and growth efficiency in the subtropical northeast Atlantic Ocean. *Limnology & Oceanography*, *52*(2), 533–546. https://doi.org/10.4319/lo.2007.52.2.0533

Aparicio, F. L., Nieto-Cid, M., Borrull, E., Romero, E., Stedmon, C. A., Sala, M. M., et al. (2015). Microbially-mediated fluorescent organic matter transformations in the deep ocean. Do the chemical precursors matter? *Frontier in Marine Science*, *2*, 106. https://doi.org/10.3389/fmars.2015.00106

Arai, K., Wada, S., Shimotori, K., Omori, Y., & Hama, T. (2018). Production and degradation of fluorescent dissolved organic matter derived from bacteria. *Journal of Oceanography*, *74*(1), 39–52. https://doi.org/10.1007/s10872-017-0436-y

Barton, E. D., Aristegui, J., Tett, P., Canton, M., García-Braun, J., Hernández-León, S., et al. (1998). The transition zone of the canary current upwelling region. *Progress in Oceanography*, *41*(4), 455–504. https://doi.org/10.1016/S0079-6611(98)00023-8

Belkin, N., Guy-Haim, T., Rubin-Blum, M., Lazar, A., Sisma-Ventura, G., Kiko, R., et al. (2022). Influence of cyclonic and anti-cyclonic eddies on plankton biomass, activity and diversity in the southeastern Mediterranean Sea. *Ocean Science Discussions*, *18*(3), 1–56.

Benner, R., & Amon, R. M. W. (2015). The size-reactivity continuum of major bioelements in the Ocean. *Annual Review of Marine Science*, *7*(1), 185–205. https://doi.org/10.1146/annurev-marine-010213-135126

Bibby, T. S., Gorbunov, M. Y., Wyman, K. W., & Falkowski, P. G. (2008). Photosynthetic community responses to upwelling in mesoscale eddies in the subtropical North Atlantic and Pacific Oceans. *Deep-Sea Research Part II Topical Studies in Oceanography*, *55*(10–13), 1310–1320. https://doi.org/10.1016/j.dsr2.2008.01.014

Bonan, G. B., & Doney, S. C. (2018). Climate, ecosystems, and planetary futures: The challenge to predict life in Earth system models. *Science*, *359*(6375). https://doi.org/10.1126/science.aam8328

Bricaud, A., Morel, A., & Prieur, L. (1981). Absorption by dissolved organic matter of the sea (yellow substance) in the UV and visible domains. *Limnology & Oceanography*, *26*(1), 43–53. https://doi.org/10.4319/lo.1981.26.1.0043

Brussaard, C. P. D. (2004). Optimization of procedures for counting viruses by flow cytometry. *Applied and Environmental Microbiology*, *70*(3), 1506–1513. https://doi.org/10.1128/AEM.70.3.1506-1513.2004

Campanero, R., Burgoa, N., Fernández-Castro, B., Valiente, S., Nieto-Cid, M., Martínez-Pérez, A. M., et al. (2022). High-resolution variability of dissolved and suspended organic matter in the Cape Verde Frontal Zone. *Frontiers in Marine Science*, *9*. https://doi.org/10.3389/fmars.2022.1006432

Cardoso, C., Caldeira, R. M. A., Relvas, P., & Stegner, A. (2020). Islands as eddy transformation and generation hotspots: Cabo Verde case study. *Progress in Oceanography*, *184*, 102271. https://doi.org/10.1016/j.pocean.2020.102271

Carlson, C. A. (2002). Production and removal processes. In D. A. Hansell, & C. A. Carlson, (Eds.), *Chapter 4 in biogeochemistry of marine dissolved organic matter* (Vol. 805, pp. 91–151). https://doi.org/10.1016/b978-012323841-2/50006-3

Carlson, C. A., & Hansell, D. A. (2015). DOM sources, sinks, reactivity, and budgets. In D. A. Hansell & C. A. Carlson (Eds.), *Biogeochemistry of marine dissolved organic matter* (pp. 66–109). Elsevier, Academic Press.

Carrasco, R., Horstmann, J., & Körtzinger, A. (2020). Surface drifter data from Meteor cruise M160. PANGAEA. https://doi.org/10.1594/PANGAEA.918612

Catalá, T. S., Álvarez-Salgado, X. A., Otero, J., Iuculano, F., Companys, B., Horstkotte, B., et al. (2016). Drivers of fluorescent dissolved organic matter in the global epipelagic ocean. *Limnology and Oceanography*, *61*(3), 1101–1119. https://doi.org/10.1002/lno.10281

Catalá, T. S., Reche, I., Fuentes-Lema, A., Romera-Castillo, C., Nieto-Cid, M., Ortega-Retuerta, E., et al. (2015). Turnover time of fluorescent dissolved organic matter in the dark global ocean. *Nature Communication*, *6*, 1–8. https://doi.org/10.1038/ncomms6986

Chari, N. V. H. K., Keerthi, S., Sarma, N. S., Pandi, S. R., Chiranjeevulu, G., Kiran, R., & Koduru, U. (2013). Fluorescence and absorption characteristics of dissolved organic matter excreted by phytoplankton species of western Bay of Bengal under axenic laboratory condition. *Journal of Experimental Marine Biology and Ecology*, *445*, 148–155. https://doi.org/10.1016/j.jembe.2013.03.015

Chavanne, C., Flament, P., Lumpkin, R., Dousset, B., Chavanne, C., Flament, P., et al. (2002). Scatterometer observations of wind variations induced by oceanic islands: Implications for wind-driven ocean circulation. *Canadian Journal of Remote Sensing*, *28*(3), 466–474. https://doi.org/10.5589/m02-047

Chelton, D. B., Gaube, P., Schlax, M. G., Early, J. J., & Samelson, R. M. (2011). The influence of nonlinear mesoscale eddies on near-surface oceanic chlorophyll. *Science*, *334*(6054), 328–333. https://doi.org/10.1126/science.1208897

Chiranjeevulu, G., Murty, K. N., Sarma, N. S., Kiran, R., Chari, N. V. H. K., Pandi, S. R., et al. (2014). Colored dissolved organic matter signature and phytoplankton response in a coastal ecosystem during mesoscale cyclonic (cold core) eddy. *Marine Environmental Research Journal*, *98*, 49–59. https://doi.org/10.1016/j.marenvres.2014.03.002

Coble, P. G. (1996). Characterization of marine and terrestrial DOM in seawater using excitation-emission matrix spectroscopy. *Marine Chemistry*, *51*(4), 325–346. https://doi.org/10.1016/0304-4203(95)00062-3

Coble, P. G. (2007). Marine optical biogeochemistry: The chemistry of ocean color. *Chemical Reviews*, *107*(2), 402–418. https://doi.org/10.1021/cr050350

Collos, Y. (1986). Time-lag algal growth dynamics: Biological constraints on primary production in aquatic environments. *Marine Ecology Progress Series*, *33*(2), 193–206. https://doi.org/10.3354/meps033193

Couespel, D., Lévy, M., & Bopp, L. (2021). Oceanic primary production decline halved in eddy-resolving simulations of global warming. *Biogeosciences*, *18*(14), 4321–4349. https://doi.org/10.5194/bg-18-4321-2021

D'Asaro, E. A. (1988). Generation of submesoscale vortices: A new mechanism. *Journal of Geophysical Research*, *93*(C6), 6685–6693. https://doi.org/10.1029/JC093iC06p06685

Devresse, Q., Becker, K. W., Bendinger, A., Hahn, J., & Engel, A. (2022). Eddy enhanced primary production accelerates bacterial growth in the Eastern Tropical North Atlantic. *Biogeosciences*, *19*(22), 5199–5219. https://doi.org/10.5194/bg-19-5199-2022

Dickson, A. G., Sabine, C. L., & Christian, J. R. (2007). *Guide to best practices for ocean CO_2 measurements* (Vol. 3, p. 191). PICES Special Publication.

Dilmahamod, A. F., Karstensen, J., Dietze, H., Löptien, U., & Fennel, K. (2022). Generation mechanisms of mesoscale eddies in the Mauritanian upwelling region. *Journal of Physical Oceanography*, *52*(1), 161–182. https://doi.org/10.1175/JPO-D-21-0092.1

Dittmar, T., Cherrier, J., & Ludwichowski, K. U. (2009). The analysis of amino acids in seawater. In O. Wurl (Ed.), *Practical guidelines for the analysis of seawater*. CRC Press. ISBN: 978-1-4200-7306-5.

Engel, A., & Galgani, L. (2016). The organic sea-surface microlayer in the upwelling region off the coast of Peru and potential implications for air-sea exchange processes. *Biogeosciences*, *13*(4), 989–1007. https://doi.org/10.5194/bg-13-989-2016

Engel, A., Händel, N., Wohlers, J., Lunau, M., Grossart, H. P., Sommer, U., & Riebesell, U. (2011). Effects of sea surface warming on the production and composition of dissolved organic matter during phytoplankton blooms: Results from a mesocosm study. *Journal of Plankton Research*, *33*(3), 357–372. https://doi.org/10.1093/plankt/fbq122

Engelstaedter, S., & Washington, R. (2007). Atmospheric controls on the annual cycle of North African dust. *Journal of Geophysical Research Atmospheres*, *112*(3), D03103. https://doi.org/10.1029/2006JD007195

Evans, C. A., O'Reily, J. E., & Thomas, J. P. (1987). *A handbook for measurement of Chl a* and primary production. Texas A and M University.

Ewart, C. S., Meyers, M. K., Wallner, E. R., McGillicuddy, D. J., & Carlson, C. A. (2008). Microbial dynamics in cyclonic and anticyclonic mode-water eddies in the northwestern Sargasso Sea. *Deep Sea Research Part II*, *55*(10–13), 1334–1347. https://doi.org/10.1016/j.dsr2.2008.02.013

Fischer, T., Karstensen, J., Dengler, M., & Bendinger, A. (2021). Multiplatform observation of cyclonic eddies during the REEBUS experiment. In *vEGU21, the 23rd EGU General Assembly, held online 19–30 April, 2021*.

Fox, B. G., Thorn, R. M. S., Anesio, A. M., & Reynolds, D. M. (2017). The in situ bacterial production of fluorescent organic matter; an investigation at a species level. *Water Research*, *125*, 350–359. https://doi.org/10.1016/j.watres.2017.08.040

Fukuzaki, K., Imai, I., Fukushima, K., Ishii, K.-I., Sawayama, S., & Yoshioka, T. (2014). Fluorescent characteristics of dissolved organic matter produced by bloom-forming coastal phytoplankton. *Journal of Plankton Research*, *36*(3), 685–694. https://doi.org/10.1093/plankt/fbn015

Garcia, H. E., & Gordon, L. I. (1992). Oxygen solubility in seawater-better fitting equations. *Limnology & Oceanography*, *37*(6), 1307–1312. https://doi.org/10.4319/lo.1992.37.6.1307

Garçon, C. V., Oschlies, A., Doney, S. C., Mcgillicuddy, D., & Waniek, J. (2001). The role of mesoscale variability on plankton dynamics in the North Atlantic. *Deep-Sea Research II*, *48*(10), 2199–2226. https://doi.org/10.1016/s0967-0645(00)00183-1

Gargas, E. (1975). A manual for phytoplankton primary production studies in the Baltic. *The Baltic Marine Biologists*, *2*, 88.

Garrido, J. L., Rodríguez, F., Campaña, E., & Zapata, M. (2003). Rapid separation of chlorophylls *a* and *b* and their demetallated and dephytylated derivatives using a monolithic silica C_{18} column and a pyridine-containing mobile phase. *Journal of Chromatography A*, *994*(1–2), 85–92. https://doi.org/10.1016/s0021-9673(03)00486-2

Gasol, J. M., & Del Giorgio, P. A. (2000). Using flow cytometry for counting natural planktonic bacteria and understanding the structure of planktonic bacterial communities. *Scientia Marina*, *64*(2), 197–224. https://doi.org/10.3989/scimar.2000.64n2197

Gattuso, J. P., Epitalon, J. M., Lavigne, H., & Orr, J. (2020). Seacarb: Seawater carbonate chemistry. R package version 3.2.13. Retrieved from http://CRAN.R-project.org/package=seacarb

Gent, P. R., & McWilliams, J. C. (1990). Isopycnal mixing in ocean circulation models. *Journal of Physical Oceanography*, *20*(1), 150–160. https://doi.org/10.1175/1520-0485(1990)020<0150:imiocm>2.0.co;2

Goni, G. J., & Johns, W. E. (2001). A census of North Brazil current rings observed from TOPEX/POSEIDON altimetry: 1992−1998. *Geophysical Research Letters*, *28*(1), 1–4. https://doi.org/10.1029/2000GL011717

Grasshoff, K., Kremling, K., & Ehrhardt, M. (1999). *Methods of sea-water analysis*. Wiley-VCH.

Guéguen, C., & Kowalczuk, P. (2013). Colored dissolved organic matter in frontal zones. In I. Belkin (Ed.), *Chemical oceanography of the frontal zones*, *The Handbook of Environmental Chemistry*. Springer Berlin Heidelberg. https://doi.org/10.1007/698_2013_244

Hansell, D. A., Carlson, C. A., Repeta, D. J., & Schlitzer, R. (2009). Dissolved organic matter in the ocean a controversy stimulates new insights. *Oceanography*, *22*(4), 202–211. https://doi.org/10.5670/oceanog.2009.109

Hayase, K., & Shinozuka, N. (1995). Vertical distribution of fluorescent organic matter along with AOU and nutrients in the equatorial Central Pacific. *Marine Chemistry*, *48*(3–4), 283–290. https://doi.org/10.1016/0304-4203(94)00051-e

Heller, I. M., Wuttig, K., & Croot, L. P. (2016). Identifying the sources and sinks of CDOM/FDOM across the Mauritanian shelf and their potential role in the decomposition of superoxide (O_2^-). *Frontiers in Marine Science*, *3*, 132. https://doi.org/10.3389/fmars.2016.00132

Helms, J. R., Stubbins, A., Perdue, E. M., Green, N. W., Chen, H., & Mopper, K. (2013). Photochemical bleaching of oceanic dissolved organic matter and its effect on absorption spectral slope and fluorescence. *Marine Chemistry*, *155*, 81–91. https://doi.org/10.1016/j.marchem.2013.05.015

Herman, J. R., Krotkov, N., Celarier, E., Larko, D., & Labow, G. (1999). Distribution from of UV radiation at the Earth's surface from TOMS-measured UV backscattered radiances. *Journal of Geophysical Research*, *104*, 12059–12076.

Hernes, P. J., & Benner, R. (2003). Photochemical and microbial degradation of dissolved lignin phenols: Implications for the fate of terrigenous dissolved organic matter in marine environments. *Journal of Geophysical Research: Oceans*, *108*(C9), 3291. https://doi.org/10.1029/2002jc001421

Hudson, N., Baker, A., Ward, D., Reynolds, D. M., Brunsdon, C., Carliell-Marquet, C., & Browning, S. (2008). Can fluorescence spectrometry be used as a surrogate for the biochemical oxygen demand (BOD) test in water quality assessment? An example from South West England. *Science of the Total Environment*, *391*(1), 149–158. https://doi.org/10.1016/j.scitotenv.2007.10.054

Ihaka, R., & Gentleman, R. (1996). R: A language for data analysis and graphics. *Journal of Computational & Graphical Statistics*, *5*(3), 299–314. https://doi.org/10.2307/1390807

Jørgensen, L., Stedmon, C. A., Granskog, M. A., & Middelboe, M. (2014). Tracing the long-term microbial production of recalcitrant fluorescent dissolved organic matter in seawater. *Geophysical Research Letter*, *41*(7), 2481–2488. https://doi.org/10.1002/2013GL058987

Jørgensen, L., Stedmon, C. A., Kragh, T., Markager, S., Middelboe, M., & Søndergaard, M. (2011). Global trends in the fluorescence characteristics and distribution of marine dissolved organic matter. *Marine Chemistry*, *126*(1–4), 139–148. https://doi.org/10.1016/j.marchem.2011.05.002

Kirchman, D., K'nees, E., & Hodson, R. (1985). Leucine incorporation and its potential as a measure of protein synthesis by bacteria in natural aquatic systems. *Applied and Environmental Microbiology*, *49*(3), 599–607. https://doi.org/10.1128/aem.49.3.599-607.1985

Klenz, T., Dengler, M., & Brandt, P. (2018). Seasonal variability of the Mauritania current and hydrography at 18°N. *Journal of Geophysical Research: Oceans*, *123*(11), 8122–8137. https://doi.org/10.1029/2018JC014264

Kowalczuk, P., Tilstone, G. H., Zabłocka, M., Röttgers, R., & Thomas, R. (2013). Composition of dissolved organic matter along an Atlantic Meridional Transect from fluorescence spectroscopy and parallel factor analysis. *Marine Chemistry*, *157*, 170–184. https://doi.org/10.1016/j.marchem.2013.10.004

Kravchenko, A., & Bullock, D. G. (1999). A comparative study of interpolation methods for mapping soil properties. *Agronomy Journal*, *91*(3), 393–400. https://doi.org/10.2134/agronj1999.00021962009100030007x

Lee, S., Wolberg, G., & Shin, S. Y. (1997). Scattered data interpolation with multilevel b-splines. *IEEE Transactions on Visualization and Computer Graphics*, *3*(3), 228–244. https://doi.org/10.1109/2945.620490

Le Vu, B., Stegner, A., & Arsouze, T. (2018). Angular Momentum Eddy Detection and tracking Algorithm (AMEDA) and its application to coastal eddy formation. *Journal of Atmospheric and Oceanic Technology*, *35*(4), 739–762. https://doi.org/10.1175/jtech-d-17-0010.1

Li, P., & Jin, H. (2017). Utilization of UV-Vis spectroscopy and related data analyses for dissolved organic matter (DOM) studies: A review. *Critical Reviews in Environmental Science and Technology*, *47*(3), 131–154. https://doi.org/10.1080/10643389.2017.1309186

Lindroth, P., & Mopper, K. (1979). High performance liquid chromatographic determination of subpicomole amounts of amino acids by precolumn fluorescence derivatization with o-phthaldialdehyde. *Analytical Chemistry*, *51*(11), 1667–1674. https://doi.org/10.1021/ac50047a019

Lochte, K., & Pfannkuche, O. (1987). Cyclonic cold-core eddy in the eastern North Atlantic. II. Nutrients, phytoplankton and bacterioplankton. *Marine Ecology Progress Series*, *39*, 153–164. https://doi.org/10.3354/meps039153

Loginova, A. N., Borchard, C., Meyer, J., Hauss, H., Kiko, R., & Engel, A. (2015). Effects of nitrate and phosphate supply on chromophoric and fluorescent dissolved organic matter in the Eastern Tropical North Atlantic: A mesocosm study. *Biogeosciences*, *12*(23), 6897–6914. https://doi.org/10.5194/bg-12-6897-2015

Loginova, A. N., Thomsen, S., & Engel, A. (2016). Chromophoric and fluorescent dissolved organic matter in and above the oxygen minimum zone off Peru. *Journal of Geophysical Research: Oceans*, *121*(11), 7973–7990. https://doi.org/10.1002/2016JC011906

Lønborg, C., Middelboe, M., & Brussaard, C. P. (2013). Viral lysis of *Micromonas pusilla*: Impacts on dissolved organic matter production and composition. *Biogeochemistry*, *116*(1–3), 231–240. https://doi.org/10.1007/s10533-013-9853-1

Lønborg, C., Yokokawa, T., Herndl, G. J., & Antón Álvarez-Salgado, X. (2015). Production and degradation of fluorescent dissolved organic matter in surface waters of the eastern North Atlantic Ocean. *Deep-Sea Research Part I: Oceanographic Research Papers*, *96*, 28–37. https://doi.org/10.1016/j.dsr.2014.11.001

López-Urrutia, Á., & Morán, X. A. G. (2007). Resource limitation of bacterial production distorts the temperature dependence of oceanic carbon cycling. *Ecology*, *88*(4), 817–822. https://doi.org/10.1890/06-1641

Lovecchio, E., Gruber, N., & Münnich, M. (2018). Mesoscale contribution to the long-range offshore transport of organic carbon from the Canary Upwelling System to the open North Atlantic. *Biogeosciences*, *15*(16), 5061–5091. https://doi.org/10.5194/bg-15-5061-2018

Maie, N., Scully, N. M., Pisani, O., & Jaffé, R. (2007). Composition of a protein-like fluorophore of dissolved organic matter in coastal wetland and estuarine ecosystems. *Water Research*, *41*(3), 563–570. https://doi.org/10.1016/j.watres.2006.11.006

Marie, D., Brussaard, C. P. D., Thyrhaug, R., Bratbak, G., & Vaulot, D. (1999). Enumeration of marine viruses in culture and natural samples by flow cytometry. *Applied and Environmental Microbiology*, *65*(1), 45–52. https://doi.org/10.1128/aem.65.1.45-52.1999

Martínez-Pérez, A. M., Catalá, T. S., Nieto-Cid, M., Otero, J., Álvarez, M., Emelianov, M., et al. (2019). Dissolved organic matter (DOM) in the open Mediterranean Sea. II: Basin-wide distribution and drivers of fluorescent DOM. *Progress in Oceanography*, *170*, 93–106. https://doi.org/10.1016/j.pocean.2018.10.019

McGillicuddy, D. J. (2016). Mechanisms of physical-biological-biogeochemical interaction at the oceanic mesoscale. *Annual Review of Marine Science*, *8*, 125–159. https://doi.org/10.1146/annurev-marine-010814-015606

Miranda, M. L., Osterholz, H., Giebel, H. A., Bruhnke, P., Dittmar, T., & Zielinski, O. (2020). Impact of UV radiation on DOM transformation on molecular level using FT-ICR-MS and PARAFAC. *Spectrochimica Acta Part A: Molecular and Biomolecular Spectroscopy*, *230*, 118027. https://doi.org/10.1016/j.saa.2020.118027

Mittelstaedt, E. (1983). The upwelling area off northwest Africa—A description of phenomena related to coastal upwelling. *Progress in Oceanography*, *12*(3), 307–331. https://doi.org/10.1016/0079-6611(83)90012-5

Mittelstaedt, E. (1991). The ocean boundary along the northwest African coast: Circulation and oceanographic properties at the sea surface. *Progress in Oceanography*, *26*(4), 307–355. https://doi.org/10.1016/0079-6611(91)90011-A

Molemaker, M. J., McWilliams, J. C., & Dewar, W. K. (2015). Submesoscale generation of mesoscale anticyclones near a separation of the California Undercurrent. *Journal of Physical Oceanography*, *45*, 613–629. https://doi.org/10.1175/JPO-D-13-0225.1

Moore, C. M., Mills, M. M., Arrigo, K. R., Berman-Frank, I., Bopp, L., & Boyd, P. W. (2013). Processes and patterns of oceanic nutrient limitation. *Nature Geoscience*, *6*(9), 701–710. https://doi.org/10.1038/ngeo1765

Mouriño-Carballido, B. (2009). Eddy-driven pulses of respiration in the Sargasso Sea. *Deep-Sea Research Part I Oceanographic Research Papers*, *56*(8), 1242–1250. https://doi.org/10.1016/j.dsr.2009.03.001

Mouriño-Carballido, B., & McGillicuddy, D. J. (2006). Mesoscale variability in the metabolic balance of the Sargasso Sea. *Limnology & Oceanography*, *51*(6), 2675–2689. https://doi.org/10.4319/lo.2006.51.6.2675

Murphy, K. R., Butler, K. D., Spencer, R. G. M., Stedmon, C. A., Boehme, J. R., & Aiken, G. R. (2010). Measurement of dissolved organic matter fluorescence in aquatic environments: An interlaboratory comparison. *Environmental Science and Technology*, *44*(24), 9405–9412. https://doi.org/10.1021/es102362t

Murphy, K. R., Ruiz, G., Coble, P., Boehme, J., & Field, P. (2004). *Mid-ocean ballast water exchange: Approach and methods for verification*. U.S. Coast Guard Research and Development Center.
Nelson, N. B., & Siegel, D. A. (2013). The global distribution and dynamics of chromophoric dissolved organic matter. *Annual Review of Marine Science*, *5*(1), 447–476. https://doi.org/10.1146/annurev-marine-120710-100751
Nielsen, E. S. (1952). The use of radio-active carbon (C14) for measuring organic production in the sea. *ICES Journal of Marine Science*, *18*(2), 117–140. https://doi.org/10.1093/icesjms/18.2.117
Nieto-Cid, M., Álvarez-Salgado, X. A., & Pérez, F. F. (2006). Microbial and photochemical reactivity of fluorescent dissolved organic matter in a coastal upwelling system. *Limnology & Oceanography*, *51*(3), 1391–1400. https://doi.org/10.4319/lo.2006.51.3.1391
Omori, Y., Saeki, A., Wada, S., Inagaki, Y., Hama, T., & Nelson, N. B. (2020). Experimental analysis of diurnal variations in humic-like fluorescent dissolved organic matter in surface seawater. *Frontier in Marine Science*, *7*, 589064. https://doi.org/10.3389/fmars.2020.589064
Ortega-Retuerta, E., Devresse, Q., Caparros, J., Marie, B., Crispi, O., Catala, P., et al. (2021). Dissolved organic matter released by two marine heterotrophic bacterial strains and its bioavailability for natural prokaryotic communities. *Environmental Microbiology*, *23*(3), 1363–1378. https://doi.org/10.1111/1462-2920.15306
Parikka, K. J., Le Romancer, M., Wauters, N., & Jacquet, S. (2017). Deciphering the virus-to-prokaryote ratio (VPR): Insights into virus-host relationships in a variety of ecosystems. *Biological Reviews*, *92*(2), 1081–1100. https://doi.org/10.1111/brv.12271
Pelegrí, J. L., & Peña-Izquierdo, J. (2015). Eastern boundary currents off North-West Africa. In L. Valdés & I. Déniz-González (Eds.), *Oceanographic and biological features in the canary current large marine ecosystem*, *IOC Technical Series* (Vol. 115, pp. 81–92). IOC-UNESCO.
Pucher, M., Wünsch, U., Weigelhofer, G., Murphy, K., Hein, T., & Graeber, D. (2019). StaRdom: Versatile software for analyzing spectroscopic data of dissolved organic matter R. *Water*, *11*(11), 1–19. https://doi.org/10.3390/w11112366
Pytkowicz, R. M. (1971). On the apparent oxygen utilization and the preformed phosphate in the oceans. *Limnology & Oceanography*, *16*(1), 39–42. https://doi.org/10.4319/lo.1971.16.1.0039
Redfield, A. C. (1942). The processes determining the concentration of oxygen, phosphate and other organic derivatives within the depths of the Atlantic Ocean. In *Papers in physical oceanography and meteorology* (Vol. 9, p. 22). Massachusetts Institute of Technology and Woods Hole Oceanographic Institution.
Redfield, A. C., Ketchum, B. H., & Richards, F. A. (1963). *The influence of organisms on the composition of the sea water*. In M. N. Hill (Ed.), The sea (Vol. 2, pp. 26–77). Interscience Publishers.
Regaudie-De-Gioux, A., & Duarte, C. M. (2012). Temperature dependence of planktonic metabolism in the ocean. *Global Biogeochemical Cycles*, *26*(1), GB1015. https://doi.org/10.1029/2010GB003907
Romera-Castillo, C., Hansell, D., & Letscher, R. (2016). New nutrients exert fundamental control on dissolved organic carbon accumulation in the surface Atlantic Ocean. *Proceedings of the National Academy of Sciences of the United States of America*, *113*(38), 10497–10502. https://doi.org/10.1073/pnas.1605344113
Romera-Castillo, C., Sarmento, H., Álvarez-Salgado, X. A., Gasol, J. M., & Marrasé, C. (2010). Production of chromophoric dissolved organic matter by marine phytoplankton. *Limnology & Oceanography*, *55*(1), 446–454. https://doi.org/10.4319/lo.2010.55.1.0446
Romera-Castillo, C., Sarmento, H., Alvarez-Salgado, X. A. Á., Gasol, J. M., & Marrasé, C. (2011). Net production and consumption of fluorescent colored dissolved organic matter by natural bacterial assemblages growing on marine phytoplankton exudates. *Applied and Environmental Microbiology*, *77*(21), 7490–7498. https://doi.org/10.1128/AEM.00200-11
Roy, S., Llewellyn, C. A., Egeland, E. S., & Johnsen, G. (Eds.) (2011). *Phytoplankton pigments: Characterization, chemotaxonomy and application in oceanography*. Cambridge University Press.
Sánchez-Pérez, E. D., Marín, I., Nunes, S., Aparicio, F. L., Fernández-González, L., Peters, F., et al. (2016). Aerosol inputs affect the optical signatures of dissolved organic matter in NW Mediterranean coastal waters. *Scientia Marina*, *80*(4), 437–446. https://doi.org/10.3989/scimar.04318.20B
Schütte, F., Brandt, P., & Karstensen, J. (2016). Occurrence and characteristics of mesoscale eddies in the tropical northeastern Atlantic Ocean. *Ocean Science*, *12*(3), 663–685. https://doi.org/10.5194/os-12-663-2016
Serret, P., Robinson, C., Aranguren-Gassis, M., García-Martín, E. E., Gist, N., Kitidis, V., et al. (2015). Both respiration and photosynthesis determine the scaling of plankton metabolism in the oligotrophic ocean. *Nature Communications*, *6*, 1–10. https://doi.org/10.1038/ncomms7961
Shimotori, K., Omori, Y., & Hama, T. (2009). Bacterial production of marine humic-like fluorescent dissolved organic matter and its biogeochemical importance. *Aquatic Microbial Ecology*, *58*, 55–66. https://doi.org/10.3354/ame01350
Shimotori, K., Watanabe, K., & Hama, T. (2012). Fluorescence characteristics of humic-like fluorescent dissolved organic matter produced by various taxa of marine bacteria. *Aquatic Microbial Ecology*, *65*(3), 249–260. https://doi.org/10.3354/ame01552
Simon, M., & Azam, F. (1989). Protein content and protein synthesis rates of planktonic marine bacteria. *Marine Ecology Progress Series*, *51*, 201–213. https://doi.org/10.3354/meps051201
Singh, A., Gandhi, N., Ramesh, R., & Prakash, S. (2015). Role of cyclonic eddy in enhancing primary and new production in the Bay of Bengal. *Journal of Sea Research*, *97*, 5–13. https://doi.org/10.1016/j.seares.2014.12.002
Smith, D. C., & Azam, F. (1992). A simple, economical method for measuring bacterial protein synthesis rates in seawater using 3H-leucine. *Marine Microbial Food Webs*, *6*, 107–114.
Smyth, T. J. (2011). Penetration of UV irradiance into the global ocean. *Journal of Geophysical Research: Oceans*, *116*(11), 1–12. https://doi.org/10.1029/2011JC007183
Stedmon, C. A., & Bro, R. (2008). Characterizing dissolved organic matter fluorescence with parallel factor analysis: A tutorial. *Limnology and Oceanography: Methods*, *6*(11), 572–579. https://doi.org/10.4319/lom.2008.6.572
Stedmon, C. A., Markager, S., & Bro, R. (2003). Tracing dissolved organic matter in aquatic environments using a new approach to fluorescence spectroscopy. *Marine Chemistry*, *82*(3−4), 239–254. https://doi.org/10.1016/S0304-4203(03)00072-0
Strickland, J. D. H., & Parsons, T. R. (1968). A practical handbook of seawater analysis. *Bulletin of the Fisheries Research Board of Canada*, *167*, 1–311.
Tanaka, K., Kuma, K., Hamasaki, K., & Yamashita, Y. (2014). Accumulation of humic-like fluorescent dissolved organic matter in the Japan Sea. *Scientific Reports*, *4*, 1–7. https://doi.org/10.1038/srep05292
Teira, E., Mourino-Carballido, B., Martinez-Garcia, S., Sobrino, C., Ameneiro, J., Hernandez-Leon, S., & Vazquez, E. (2012). Primary production and bacterial carbon metabolism around South Shetland Islands in the Southern Ocean. *Deep Sea Research Part I: Oceanographic Research Papers*, *69*, 70–81. https://doi.org/10.1016/j.dsr.2012.07.002
Thomsen, S., Kanzow, T., Krahmann, G., Greatbatch, J. R., Dengler, M., & Lavik, G. S. (2016). The formation of a sub-surface anticyclonic eddy in the Peru-Chile Undercurrent and its impact on the near-coastal salinity, oxygen, and nutrient distributions. *Journal of Geophysical Research: Ocean*, *121*(1), 476–501. https://doi.org/10.1002/2015JC010878

Timko, S. A., Maydanov, A., Pittelli, S. L., Conte, M. H., Cooper, W. J., Koch, B. P., et al. (2015). Depth-dependent photodegradation of marine dissolved organic matter. *Frontiers in Marine Science*, *2*. https://doi.org/10.3389/fmars.2015.00066

Valiente, S., Fernández-Castro, B., Campanero, R., Marrero-Díaz, A., Rodríguez-Santana, A., Gelado-Cabellero, M. D., et al. (2022). Dissolved and suspended organic matter dynamics in the Cape Verde Frontal Zone (NW Africa). *Progress in Oceanography*, *201*, 102727. https://doi.org/10.1016/j.pocean.2021.102727

Wang, C., Guo, W., Li, Y., Stubbins, A., Li, Y., Song, G., et al. (2017). Hydrological and biogeochemical controls on absorption and fluorescence of dissolved organic matter in the Northern South China Sea. *Journal of Geophysical Research: Biogeosciences*, *122*(12), 3405–3418. https://doi.org/10.1002/2017JG004100

Wei, T., & Simko, V. (2021). R package 'corrplot': Visualization of a correlation matrix. Version 0.92. Retrieved from https://github.com/taiyun/corrplot

Wetz, M. S., & Wheeler, P. A. (2004). Response of bacteria to simulated upwelling phytoplankton blooms. *Marine Ecology Progress Series*, *272*, 49–57. https://doi.org/10.3354/meps272049

Wickham, H. (2016). Programming with ggplot2. In *ggplot2. Use R!*. Springer. https://doi.org/10.1007/978-3-319-24277-4_12

Williams, C. J., Yamashita, Y., Wilson, H. F., Jaffé, R., & Xenopoulos, M. A. (2010). Unraveling the role of land use and microbial activity in shaping dissolved organic matter characteristics in stream ecosystems. *Limnology & Oceanography*, *55*(3), 1159–1171. https://doi.org/10.4319/lo.2010.55.3.1159

Winkler, L. W. (1888). Die Bestimmung des im Wasser gelösten Sauerstoffes. *Berichte der Deutschen Chemischen Gesellschaft*, *21*(2), 2843–2854. https://doi.org/10.1002/cber.188802102122

Witter, D. L., & Gordon, A. L. (1999). Interannual variability of South Atlantic circulation from 4 years of TOPEX/POSEIDON satellite altimeter observations. *Journal of Geophysical Research: Oceans*, *104*(C9), 20927–20948. https://doi.org/10.1029/1999jc900023

Xiao, X., Guo, W., Li, X., Wang, C., Chen, X., Lin, X., et al. (2021). Viral lysis alters the optical properties and biological availability of dissolved organic matter derived from *Prochlorococcus* picocyanobacteria. *Applied and Environmental Microbiology*, *87*(3), e02271–e2320. https://doi.org/10.1128/aem.02271-20

Xiao, Y. H., Sara-Aho, T., Hartikainen, H., & Vähätalo, A. V. (2013). Contribution of ferric iron to light absorption by chromophoric dissolved organic matter. *Limnology & Oceanography*, *58*(2), 653–662. https://doi.org/10.4319/lo.2013.58.2.0653

Yamashita, Y., Hashihama, F., Saito, H., Fukuda, H., & Ogawa, H. (2017). Factors controlling the geographical distribution of fluorescent dissolved organic matter in the surface waters of the Pacific Ocean. *Limnology & Oceanography*, *62*(6), 2360–2374. https://doi.org/10.1002/lno.10570

Yamashita, Y., & Tanoue, E. (2003). Chemical characterization of protein-like fluorophores in DOM in relation to aromatic amino acids. *Marine Chemistry*, *82*(3–4), 255–271. https://doi.org/10.1016/S0304-4203(03)00073-2

Yamashita, Y., Tsukasaki, A., Nishida, T., & Tanoue, E. (2007). Vertical and horizontal distribution of fluorescent dissolved organic matter in the Southern Ocean. *Marine Chemistry*, *106*(3–4), 498–509. https://doi.org/10.1016/j.marchem.2007.05.004

Yan, W., Zhang, R., & Jiao, N. (2018). A longstanding complex tropical dipole shapes marine microbial biogeography. *Applied and Environmental Microbiology*, *84*(18). https://doi.org/10.1128/AEM.00614-18

Zhang, M., Wu, Y., Wang, F., Xu, D., Liu, S., & Zhou, M. (2020). Hotspot of organic carbon export driven by mesoscale eddies in the slope region of the Northern South China Sea. *Frontiers in Marine Science*, *7*, 1–13. https://doi.org/10.3389/fmars.2020.00444

Zhang, Y., Sintes, E., Chen, J., Zhang, Y., Dai, M., Jiao, N., & Herndl, G. J. (2009). Role of mesoscale cyclonic eddies in the distribution and activity of Archaea and Bacteria in the South China Sea. *Aquatic Microbial Ecology*, *56*, 65–79. https://doi.org/10.3354/ame01324

Zhu, W. Z., Yang, G. P., & Zhang, H. H. (2017). Photochemical behavior of dissolved and colloidal organic matter in estuarine and oceanic waters. *Science of the Total Environment*, *607–608*, 214–224. https://doi.org/10.1016/j.scitotenv.2017.06.163

References From the Supporting Information

McPeters, R. D., Bhartia, P. K., Krueger, A. J., Herman, J. R., & Torres, O. (1996). *Nimbus-7 total ozone mapping spectrometer (TOMS) data products user's guide*. NASA Reference Publication.

McPeters, R. D., Bhartia, P. K., Krueger, A. J., Torres, O., & Herman, J. R. (1998). *Earth probe total ozone mapping spectrometer (TOMS) data products user's guide*. NASA Technical Publication 1998−206895.